AD-A188 522 ANALYSIS OF A SERIES OF ELECTROMAGNETIC LAUNCHER FIRINGS(U) MATERIALS RESEARCH LABS ASCOT VALE (AUSTRALIA) V KOWALENKO JUN 87 MRL-R-1053 1/1

UNCLASSIFIED F/G 19/6 NL

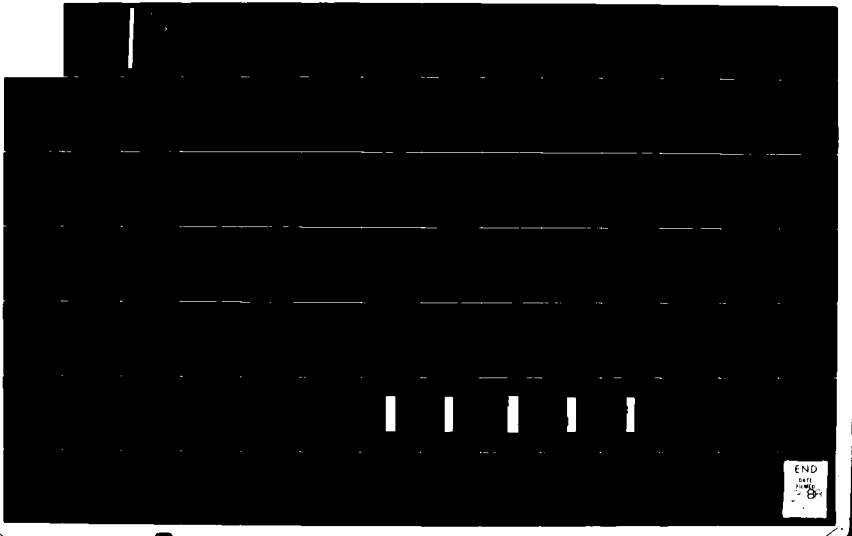

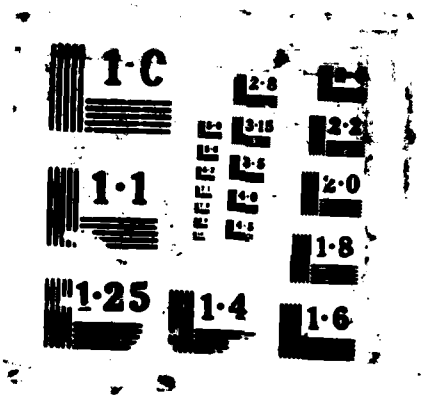
1·C
1·1
1·25
1·4
2·8
3·15
2·2
2·0
1·8
1·6

DTIC FILE COPY

(4)

MRL-R-1053

AR-005-131

DEPARTMENT OF DEFENCE

DEFENCE SCIENCE AND TECHNOLOGY ORGANISATION

MATERIALS RESEARCH LABORATORIES

MELBOURNE, VICTORIA

DTIC
ELECTE
DEC 2 3 1987
S D
D

REPORT

MRL-R-1053

AD-A188 522

ANALYSIS OF A SERIES OF ELECTROMAGNETIC LAUNCHER FIRINGS

V. Kowalenko

DISTRIBUTION STATEMENT A
Approved for public release
Distribution Unlimited

Approved for Public Release

DSTO
MARIBYRNONG

87 12 14 053

© Commonwealth of Australia

JUNE 1987

DEPARTMENT OF DEFENCE

MATERIALS RESEARCH LABORATORIES

REPORT

MRL-R-1053

ANALYSIS OF A SERIES OF ELECTROMAGNETIC LAUNCHER FIRINGS

V. Kowalenko

ABSTRACT

In this report theoretical aspects of electromagnetic launchers are presented in conjunction with an analysis of diagnostic measurements taken during the RAPID Plasma Intensity Profiles (RPIP) series of firings. These theoretical aspects deal with the current-time behaviour, the plasma temperature and the evaluation of railgun parameters such as the efficiency and effective inductance per unit length.

The principal aims of the RPIP series were: (1) to see if different types and masses of plasma-generating foils affected railgun performance and the diagnostic measurements taken during each firing and (2) to compare some of the theoretical predictions of the Plasma Armature Rail Accelerator (PARA) simulation code with experimental results.

Projectile displacement-time results for the series were obtained by digitising photographs from a streak camera and in order to verify the PARA predictions for plasma-length behaviour, light intensity profiles were produced from microdensitometer readings of the streak films.

The experimental results were affected by plasma disruption, arcing ahead of the projectile and plasma leakage. These effects are also discussed in this report.

Approved for Public Release

POSTAL ADDRESS: Director, Materials Research Laboratories
P.O. Box 50, Ascot Vale, Victoria 3032, Australia

SYMBOLS

A	cross-sectional area of the rails, m^2
a	coefficient of a quadratic curve fit, m/s^2
a_1	coefficient of a cubic curve fit, m/s^3
$\underline{B}$	magnetic field in the plasma armature, T
b	coefficient of a quadratic curve fit, m/s
b_1	coefficient of a cubic curve fit, m/s
C	capacitance of the capacitor bank, F
c	coefficient of a quadratic curve fit, m
c_1	coefficient of a cubic curve fit, m/s
d	maximum vertical extension of a ballistic pendulum, m
d_1	coefficient of a cubic curve fit, m
e	induced emf, V
E_R	energy lost due to resistive heating in the capacitively-driven stage, J
f	general force term acting against the motion of the arc-projectile system, N
f_T	time factor for the streak camera
g	acceleration due to gravity, m/s^2
h	height of the bore in a railgun, m
h_r	height of the rails, m
I	current in the railgun circuit, A
I_o	current in the railgun circuit at the instant of crowbarring of the capacitor bank, A
I_1	current passing through the plasma armature when a runaway arc appears, A
I_2	current passing through a runaway arc, A
I_d	product of the current and projectile displacement, Am
I_m	maximum current possible in a railgun circuit, A

DTIC COPY INSPECTED 1

Availability Codes
Dist | Avail and/or Special
A-1

I_p	peak current obtained during a railgun firing, A
I_t	current in the railgun circuit when the time constant begins to vary in the inductively-driven stage, A
j	current density in the plasma armature, A/m^2
k	gradient obtained from a plot of log I/I_o versus time, s^{-1}
L_o	inductance of the railgun circuit excluding the rail inductance, H
L'	rail inductance per unit length, H/m
l_a	length of the plasma armature, m
l_b	maximum horizontal displacement by the ballistic pendulum, m
L'_{eff}	effective inductance per unit length, H/m
L_p	inductance of the plasma armature, H
L'_p	propelling inductance per unit length, H/m
l_r	length of the runaway arc, m
L_{rail}	inductance of the rails, H
l_v	total vertical length on a streak photograph, m
M	magnification factor for streak photographs
m_a	mass of the plasma armature, kg
M_b	mass of the ballistic pendulum, kg
m_p	mass of the projectile, kg
m_r	mass of the runaway arc, kg
n_e	electron density of the plasma armature, m^{-3}
P	pressure in the plasma armature, Pa
p	correlation coefficient of curve fits
Q	charge on the capacitor bank at time t, C
Q_r	heat flux incident on the rails in the plasma region, $Jm^{-2}s^{-1}$
R	resistance of the busbars and plasma-armature, Ω
R_1	total circuit resistance in the inductively-driven stage, Ω

$\dot{R}$	resistance increase per unit time occurring late in the inductively-driven stage, Ω/s
R'	resistance per unit length of the rails, Ω/m
R_a	resistance of the plasma armature, Ω
R_r	resistance of the runaway arc, Ω
R_{rail}	resistance of the rails, Ω
R_{S_1}	resistance of the main switch, S_1, Ω
R_{S_2}	resistance of the switch S_2 in a RAPID railgun, Ω
R_{tot}	total resistance of a railgun circuit for the capacitively-driven stage, Ω
T	average internal temperature of the plasma armature, K
t	time from shot-start, s
t_c	time at which crowbarring of the capacitor banks occurs with respect to shot-start, s
t_e	exit time of the projectile with respect to shot-start, s
t_f	total event time measured on a streak photograph, s
t_{max}	the time at which peak current occurs with respect to shot-start, s
U_a	volume of the plasma armature, m^3
V	voltage of the capacitor bank, V
v	velocity of the arc-projectile system, m/s
V_o	initial voltage of the capacitor bank, V
v_e	exit velocity of the projectile, m/s
V_{el}	sum of the rail-electrode drops, V
V_M	voltage measured across the muzzle, V
v_{max}	maximum possible velocity of the projectile, m/s
V_r	sum of the electrode drops across the runaway arc, V
w	separation width of the rails or bore-width, m
x	displacement of the arc-projectile system, m
x_1	degree of first ionisation in a plasma

x_2	degree of second ionisation in a plasma
Z	dimensionless parameter appearing in the Spitzer expression for plasma resistivity
α	degree of ionisation in a plasma
β	factor relating the energy stored initially in the capacitor bank to the energy stored by the inductor at peak current
γ	a parameter given by Equation (50), s
γ_E	a parameter appearing in the Spitzer expression for resistivity dependent on the degree of ionisation
Δt	life-time of a runaway arc, s
ϵ_{max}	upper bound for the efficiency of a railgun
η_a	resistivity of the plasma armature, Ωm
η_r	resistivity of the runaway arc, Ωm
η_{rail}	average resistivity of one rail, Ωm
κ	ratio of rail voltage term in Equation (61) to the runaway arc's potential
σ	electrical conductivity, $\Omega^{-1}m^{-1}$
σ_s	Stefan's constant, 5.67×10^{-8} $Jm^{-2}K^{-4}s^{-1}$
τ	time constant in the inductively-driven stage, s
ω	angular resonant frequency for the capacitively-driven stage, rad/s

C O N T E N T S

ANALYSIS OF A SERIES OF ELECTROMAGNETIC LAUNCHER FIRINGS

1. INTRODUCTION

A series of electromagnetic launcher firings known as the RAPID Plasma Intensity Profiles (RPIP) Series was conducted at Materials Research Laboratories (MRL) in 1983. In the series, different masses and types of metallic foil were used to generate the plasma armatures within the launcher or railgun. The aim of this report is to present a detailed analysis of the various diagnostic measurements taken during each firing in the RPIP series.

RAPID, an acronym for Railgun Armature Plasma Investigation Device, was the type of closed breech railgun design [1] used in the RPIP series. A special feature of this railgun design was that optical photography of the events occurring in the bore during acceleration could be carried out because the rails were encased in a transparent polycarbonate gun-body.

In the RPIP series both streak and framing cameras were used to photograph the events occurring in the bore of the electromagnetic launcher. The streak films were analysed in a micro-densitometer and yielded the light intensity profiles of the plasma armature for the first time in firings at MRL.

The total number of firings in the RPIP series was 26. Foils made of aluminium, copper and zinc were used to generate plasma armatures. For each foil type three different masses were used. It was also planned that each firing would be repeated at least once in order to check the reliability of the results obtained throughout the series. Thus a total of 18 firings was initially considered necessary for the successful completion of the series. However, during the series, anomalous effects such as plasma leakage, arcing ahead of the projectile and disruption within the plasma armature occurred. Plasma leakage and arcing ahead of the projectile were most likely to occur when the gun-bodies had eroded severely, particularly near the breech. In an attempt to overcome these effects, the RAPID gun-bodies were removed and then turned end for end. Hence, the number of firings

was extended so that the series might be completed successfully. However, it became apparent after 26 firings that it was no longer possible to prevent the anomalous effects, so the series was terminated.

The contents of this report are arranged as follows. In Section 2 some necessary background information concerned with the predictions of the Plasma Armature Rail Accelerator (PARA) railgun simulation code is presented. Some of the aims of the RPIP series evolved from the predictions of the PARA code. The aims of the RPIP series are then presented in Section 3 with the experimental details for the series appearing in Section 4. In Section 5, experimental results and observations are discussed. The results for the exit-velocities are presented in Subsection 5.1 and then an analysis of the current-time records follows in Subsection 5.2. Also in Subsection 5.2, the energy loss during the capacitively-driven stage is investigated. The streak photography and muzzle voltage records are discussed in Subsections 5.3 and 5.4, respectively. The displacement-time results obtained from digitising the streak photographs and the velocity data for RPIP experiment No. 2 (RPIP02) are analysed in Subsections 5.5 and 5.6. Estimates for the length and average internal temperature of the plasma armature using the results of the microdensitometer readings are then given in Subsections 5.7 and 5.8 followed by a short discussion in Subsection 5.9 concerning damage to the rails. In Section 6, three different railgun parameters are examined. The first of these parameters is the railgun efficiency, which is derived theoretically in Subsection 6.1. Using the theoretical expressions in Subsection 6.1, a lower bound for the effective inductance per unit length is found in Subsection 6.2. The remaining railgun parameter, the effective inductance per unit length divided by the total mass of the plasma armature and projectile, is discussed in conjunction with retardational effects in Subsection 6.3. In Section 7, the anomalous effect of arcing ahead of the projectile is examined from a theoretical viewpoint. The results relevant to some of the aims of the RPIP series are then discussed in Section 8. In the concluding Section 9, a summary of the results of the RPIP series is presented.

2. BACKGROUND

Railgun performance is an expression used by railgun workers to denote the acceleration, velocity and displacement of the plasma-projectile system during a railgun firing. Since it is the aim of electromagnetic launchers to accelerate projectiles to significantly higher velocities than previously attained by conventional guns, the most important railgun performance characteristic is the velocity of the plasma-projectile system, particularly on exit.

The PARA railgun simulation code developed by Thio [2] combined the prediction of railgun performance with the prediction of detailed physical properties of the plasma-armature. As a simplification, some of the time-varying properties of the plasma armature were obtained by using a quasi-static approach. The most important physical properties of the plasma armature evaluated by the PARA code were the average temperature, pressure, volume and degree of ionisation. Values for these physical quantities were

required for determining both the electrical resistivity and resistance of the plasma armature.

The electrical resistance of the plasma armature was required in the PARA code as a parameter in the Kirchhoff equation for the railgun circuit. The railgun current was determined from the Kirchhoff equation and then introduced into the equation of motion for the plasma-projectile system in a railgun. Thus it was necessary to combine the predictions of railgun performance with the predictions of the detailed physical properties of the plasma armature.

In the PARA code the plasma length was obtained by dividing the plasma volume by cross-sectional area of the railgun bore. This was not an unreasonable assumption because spectroscopic studies of the railgun muzzle flash [3] revealed that the plasma armature did interact with its walls, thereby indicating that the plasma armature was bounded by the cross-sectional area of the bore along some, if not all, of its length. The PARA code's prediction for the general behaviour of the plasma length during a firing could be compared with length measurements obtained from microdensitometer readings of the streak film. The plasma length was found by measuring the length over which the intensity of the plasma armature exceeded the background intensity on the readings.

The general predictions for railgun performance produced by the PARA code can also be checked with experiment. Richardson and Marshall [4] have compared the railgun performance predictions of the PARA code directly with the experimental results obtained in the series using the railgun type ERGS-1M [5,6]. They found that if the mass of the aluminium foil used to generate the plasma armature for a 3 kV firing with the ERGS-1M railgun was 0.0104 g, then the projectile's exit velocity predicted by the PARA code would range from 750 m/s to 800 m/s depending on the values chosen for the resistances of the railgun circuit and for the electrode potential drops. Since different values for the electrode potential drops and for the resistance of the railgun circuit affected the predictions for the projectile's exit velocity only marginally, Richardson and Marshall chose to use the values which would predict an exit velocity of 800 m/s to compute the results for an aluminium-foil mass of 0.036 g. They found that the predicted exit velocity was 1225 m/s. Thus an increase by a factor of 3 in the foil mass would result in an increase of over 50% in projectile exit velocity. For a capacitor bank voltage of 7 kV, Richardson and Marshall computed exit velocities of 2050 and 1875 m/s for foil masses of 0.036 and 0.0104 g respectively. The PARA code therefore predicts that a railgun can become more efficient using heavier foil masses for some values of input energies. The range of foil masses over which this behaviour would apply was never determined.

Although the RAPID railgun for the RPIP series was different from the ERGS-1M railgun, the input energy for the RPIP series was chosen to be close to the input energy of a 3 kV firing using the ERGS-1M railgun. Thus the behaviour predicted by the PARA code concerning various foil masses could be checked with experiment.

The masses of aluminium foil used in the RPIP series were 0.002, 0.012 and 0.062 g. Therefore the range of aluminium foil masses for the

RPIP series extended above and below the range considered by Richardson and Marshall. Hence, if the PARA code's prediction concerning foil masses was correct, then significant variation in the projectile's exit velocity would be expected in the RPIP series with the exit velocities being substantially greater for those firings involving the heavier pieces of metallic foil.

3. AIMS OF THE SERIES

The primary aims of the RPIP series were:

(1) to study the effect of different types and masses of plasma-generating metallic foil on railgun performance,

(2) to observe the effect of different types and masses of foils on the diagnostic measurements taken during each firing, and

(3) to compare the PARA code's predictions concerning the projectile's exit velocity and the behaviour of the plasma length with the experimental results.

A number of secondary aims arose from the primary aims. To obtain data for the displacement of the projectile during a firing, the plasma was photographed over the duration of each firing. The secondary aims which followed as a result of photographing the plasma armature were:

(1) to study the stability and uniformity of the plasma armature,

(2) to obtain estimates of the plasma armature length, and

(3) to obtain estimates of the average internal temperature of the plasma armature using the plasma length estimates.

There were some additional secondary aims, which followed from the second primary aim and these were:

(1) to study the effect of the different masses and types of plasma generating foil on the muzzle and breech voltage records,

(2) to study the current-time behaviour and its dependence on the different foil parameters, and

(3) to study rail damage.

In this report the three primary aims are discussed extensively in section 8 whereas the secondary aims are discussed in the various subsections comprising section 5. As mentioned previously, this report will also include various theoretical aspects concerned with electromagnetic launchers in general which arose during the analysis of the RPIP results.

4. EXPERIMENTAL DETAILS

In previous firings conducted at MRL [5,6], projectile displacement-time data were obtained by placing small magnetic flux-probes at various positions along the gun-body with their orientation axes parallel to the projectile's direction of motion. The use of these probes led to problems because there were not enough discrete recording stations/channels available to obtain a substantial number of displacement-time results. From streak photography a much greater number of displacement-time data could be obtained than previously, so that a more thorough analysis could be undertaken.

Projectile displacement-time data were obtained from the streak photographs using a Calcomp digitiser and these data were transferred to a VAX 11/780 computer. Using the GRAPH computer code developed by Kennett [7], the data were plotted by a Tektronix 4662 plotter. Amongst its many capabilities, the GRAPH program provides a curve-fitting routine, which was used to analyse some of the experimental data.

All of the firings in the RPIP series were done with high-speed streak and framing photography set up to record the most intense features of the plasma armature [8]. The photographs obtained from the film of the frame camera showed more detail than the streak photographs because the neutral density filter on the streak camera was 10 times less dense than that on the frame camera throughout the series. The streak camera was positioned so that the lenses and slit were set up to observe detail in the length direction of the gun-body (i.e. the direction of projectile motion) and in the width-direction of the railgun bore.

Microdensitometer readings of many of the streak films were taken at various positions in the direction of projectile motion. These readings yielded profiles of the light intensity over the length of the plasma armature. Plasma length measurements could then be determined from each plasma intensity-profile by measuring the distance between the points where the plasma intensity dropped to the background intensity-level. In addition, the six or seven microdensitometer readings performed for each experiment provided displacement-time results, which served as a check on the results obtained from the digitiser.

The power source [1,5] for the electromagnetic launcher used in the RPIP series consisted of a capacitor bank connected in series with a storage inductor via a spark-gap switch. This switch was responsible for turning on the main discharge. The capacitor bank was equipped with a crowbar switch designed to shunt the current once the energy had been transferred to the storage inductor. The capacitance of the capacitor bank was measured as $1597 \pm 16\ \mu F$ before the commencement of the the series. The inductance of the storage inductor was measured as $6.3 \pm 0.3\ \mu H$. In all of the firings reported here the capacitor bank was charged to 6.00 ± 0.03 kV.

The cadmium-copper rails used in the RAPID railgun were 0.5 m in length, 12.5 mm square in cross-section and were mounted 8 mm apart. The bore cross-section was 6 mm in height and 8 mm in width. Red-fibre projectiles, chosen because of their opacity, were used throughout the series. These

projectiles weighed about 0.38 g, were 6 mm in length and had the same cross-sectional area as the bore.

The various pieces of metallic foil used to generate the initial plasma armatures were folded and glued to the back of the projectiles. In previous firings a standard piece of aluminium foil weighing about 0.012 g and 0.025 mm thick had been folded to the dimensions of 11 x 6 x 0.1 mm. In the RPIP series two variations from the standard piece of aluminium foil were used to generate plasma armatures in addition to the standard piece. The first variation was about 1/5 the mass of the standard piece while the second was about 5 times the standard mass.

The standard zinc foil was cut to the dimensions of 44 x 6 mm from a 0.025 mm thick foil and weighed approximately 0.04 g. The standard copper foils measured 11 x 3.4 mm and were cut from 0.125 mm thick foil. These weighed about 0.05 g. The standard foil masses were selected to yield similar numbers of atoms. One fifth and five-times variations of the copper and zinc foils were also used in the series.

The time-of-arrival detection system used in the RPIP series consisted of a fibre-optic probe, a laser beam probe, a pencil-lead break and a ballistic pendulum with a breakscreen attached to it. The fibre-optic probe was situated 3 cm beyond the muzzle of the railgun and the laser beam was situated a further 30 cm from the fibre-optic probe. The pencil-lead was positioned a further 6.5 cm from the laser whilst the ballistic pendulum was situated another 123.5 cm from the breakwire.

The time-of-arrival record for the second firing in the RPIP series (RPIP02) is presented in Figure 1. After the projectile leaves the gun-barrel, the flash produced by the plasma armature immediately behind the projectile activates the fibre-optic probe which produces the first peak in Figure 1. A short time later, the laser beam is intercepted thereby producing the first minimum below the time-axis in Figure 1. The second minimum below the time-axis is produced when the projectile hits the pencil-lead break. The sudden jump or vertical line across the time axis in Figure 1 corresponds to the projectile's penetration of the breakscreen on the ballistic pendulum.

The time-of-arrival record shown in Figure 1 is an example of a successful record. However, only four of the velocity records can be considered satisfactory. In many of the experiments the plasma armature failed to activate the fibre-optic probe as in Figure 2, or the projectile missed either the pencil-lead break or the ballistic pendulum as in Figure 3. In other firings the fibre-optic probe responded early as is also shown in Figure 3. Because of these inconsistencies it was necessary to use a multi-sensor system to counter the possible failure of some of the sensors.

The exit-velocity v_e estimated from the ballistic pendulum was obtained by using the following equation:

$$v_e^2 = 2gd\,(1 + M_b/m_p)^2(1-(1-l_b^2/d^2)^{1/2}) \qquad (1)$$

where M_b was the mass of the ballistic pendulum (1740 g), m_p the mass of the projectile, g the acceleration due to gravity, d the maximum vertical extension of the pendulum (4.1 m) and l_b the measured maximum horizontal displacement from the initial position of the pendulum. This displacement was obtained through the attachment of a marker-pen to the pendulum. In general, the results obtained from the ballistic pendulum were not accurate because the ballistic pendulum was situated far from the muzzle and because on some occasions the marker-pen became loose, thereby yielding unreliable values for l_b.

In each firing, transient recorders were used to record the muzzle and breech voltages as functions of time. In addition, the current was recorded using a Rogowski belt compensated by a simple RC-integrator. All current values reported here have been processed in the manner as described by Clark and Bedford [5]. The data obtained by the transient recorders were transferred to a PDP LSI-minicomputer.

Two RAPID gun-bodies were used alternately in the RPIP series. Both gun-bodies had been used extensively in previous firings and as mentioned previously, these gun-bodies were reversed after 20 firings.

5. EXPERIMENTAL RESULTS

Throughout this report references to plasma leakage and arcing ahead of the projectile are made. Plasma leakage is defined in this report as the loss of material from the plasma armature. In the RPIP experiments most of the plasma leakage was detected ahead of the projectile. Arcing ahead of the projectile is the situation where part of the railgun current passes between the rails ahead of the projectile. The arc produced ahead of the projectile is referred to as a runaway arc and, like the main plasma arc, it is subject to a Lorentz force. It should be noted that these effects were first reported by Stainsby and Bedford [8].

A comparison of the predictions of the PARA code with the results of the RPIP experiments was difficult because the frame photographs revealed that plasma leakage occurred during each firing. Leakage is not allowed for in the PARA code because the plasma mass is assumed to be constant. However, plasma leakage did not appear on all of the streak photographs. Only those firings in which the plasma leakage was absent on the streak photographs, were compared with the predictions of the PARA code.

Another problem in comparing the PARA predictions with the RPIP results was that material produced by the melting of the rails [9] and the gun-body was introduced into the plasma armature. This behaviour has been revealed by recent spectroscopic studies [4], in which trace elements belonging to the plasma armature and railgun body have been found in the muzzle-flash of the plasma armature. In theoretical studies in this report it will be assumed that no extra material is introduced into the plasma armature during a railgun firing.

Arcing ahead of the projectile was allowed for in the PARA code because railgun performance is affected by the reduction of current in the plasma armature. When allowing for this effect in the PARA code, the user is expected to specify a constant fraction of the total railgun current passing through the runaway arc. As is discussed in Section 7, the fraction of total current being drawn away from the plasma armature is not constant when arcing occurs ahead of the projectile. Comparisons of the PARA code predictions with RPIP firings in which arcing occurred ahead of the projectile will not be made in this report.

Of the 26 firings conducted in the RPIP series there were only nine firings in which neither significant plasma leakage nor arcing ahead of the projectile was observed on the streak photographs. However, seven of those nine firings were only moderately successful because plasma breakup or disruption was apparent on the streak photographs. This effect, which is also not considered in the plasma model for the PARA code, had a marginal effect on railgun performance and is discussed in Subsection 5.1. Thus of the 26 firings, only two firings (RPIP02 and RPIP06) were free from any spurious effects degrading railgun performance.

A summary of the RPIP firings is presented in Table 1. In addition to presenting the foil type and mass for each experiment, the gun-body number is presented because both gun-bodies had been used previously in different series of firings and hence were not the same. Since runaway arcs began to appear regularly after RPIP16, it was decided to reverse the RAPID gun-bodies after RPIP20. Comments about the presence of plasma leakage, arcing ahead of the projectile and plasma breakup on the streak photograph are presented for each firing in the three remaining columns of Table 1. Comments concerning plasma leakage and breakup could not be made for RPIP14, RPIP23 and RPIP24 because the streak camera either did not record or the film was poorly developed. The comments on the non-appearance of runaway arcs in RPIP14 and RPIP24 were made by observing the breech and muzzle voltage records for these experiments. Only part of the RPIP25 firing was recorded successfully by the streak camera.

5.1 Exit Velocities

The results for the average exit-velocities calculated from the time-of-arrival records are displayed in Table 2. The second column in Table 2 lists the average velocities over the distance between the fibre-optic probe and the laser beam. The average velocities over the distance between the laser beam and the pencil-lead break are presented in the next column. The fourth column lists the average velocities over the distance between the pencil-lead and the breakscreen attached to the ballistic pendulum. In cases where the pencil-lead was not broken, the average velocity corresponding to the distance between the laser beam and the breakscreen was determined. These results appear in the fifth column of Table 2. The velocities obtained by using Equation (1) are listed in the sixth column. Comments concerning the time-of-arrival records are presented in the final column in order to explain the absence of some of the recorded velocities in the columns or to explain why some of the exit velocities were considered dubious. Those exit velocities marked with a '+' in Table 2 represent the most dubious of the results.

Examples of less successful time-of-arrival records have already been presented in Figures 2 and 3, which show the records for RPIP11 and RPIP25, respectively. In Figure 2, the response of the fibre-optic probe is not as expected because plasma leakage produced an early and uncharacteristic output from the probe. This is surprising because the streak photograph for the firing did not reveal any plasma leakage. In contrast to Figure 2, the time-of-arrival record in Figure 3 has two muzzle flash peaks. The first peak on this record has been caused by a runaway arc while the second is due to the plasma armature. In addition to the two peaks appearing in Figure 3, the record shows that the projectile failed to hit the ballistic pendulum. It should be noted that some of the observations described in this paragraph have already been reported in Reference [8].

In some firings both the breakscreen and the ballistic pendulum had two separate holes due to fragmentation of the projectile. Instances where this behaviour occurred are also listed in the comments column of Table 2. The comment 'possible fragmentation' refers to firings in which it was found that the breakscreen had two intersecting holes. It was not certain in these cases whether the projectile had fragmented on impact with the ballistic pendulum or whether the intersection of the two holes was coincidental thereby implying that the projectile had fragmented earlier. The exit velocities obtained by using Equation (1) might not be reliable for these cases.

With the exception of the flash-to-laser beam velocities in RPIP01 and in RPIP13, none of the velocities appearing in Table 2 were above 1 km/s. The flash-to-laser beam velocities for RPIP01 and RPIP13 are unreliable because in both cases there is no distinctive peak on the time-of-arrival record corresponding to the fibre-optic probe sensing the muzzle flash. In fact both time-of-arrival records are similar to the record in Figure 2.

For the projectiles used in the RPIP series, a velocity of 1 km/s corresponds to a kinetic energy of 192 J. Since the firings were carried out with stored energies of 28.7 ± 0.6 kJ in the capacitor bank, the overall system efficiency for the series was less than 0.7 percent. This result indicates that the RAPID railgun is very inefficient under the operating conditions described earlier. In Section 6 this result is shown to be consistent with the theoretical estimate of the upper bound for the efficiency of an electromagnetic launcher of this type.

The firings with the highest exit velocities were RPIP02, RPIP06, RPIP12 and RPIP21. From Table 1, it can be seen that in these firings there was negligible plasma leakage and no arcing ahead of the projectile. Although plasma breakup or disruption occurred in RPIP12 and RPIP21, it had little effect on the exit velocities and hence is not a serious effect in a RAPID railgun under the conditions of the RPIP series.

5.2 Current-Time Analysis and Inductance - Charging Energy Loss.

Figure 4 shows the current-time record for RPIP02 corrected in the manner as described in Reference [6]. The current rises sinusoidally reaching a maximum value just above 80 kA about 160 μs after shot-start. The

time at which crowbarring of the capacitor bank occurs, denoted by t_c in this report, is approximately 190 μs after shot-start. From then on, the current decays exponentially. In Figure 4 the current appears to be decreasing linearly in the inductively-driven stage because of the scale used in plotting the results. Projectile exit occurs about 790 μs after shot-start.

All of the current-time records for the RPIP series with the exception of RPIP14, RPIP21 and RPIP23 are similar to Figure 4. There were no records obtained for RPIP14 and RPIP21 because problems occurred in accessing the data from the transient recorders. In RPIP23, the crowbar switch failed and the current-time record resembled a damped oscillatory curve.

The equivalent electric circuit for the electromagnetic launcher used in the RPIP series is shown in Figure 5. Here the capacitor bank C is connected in series with a storage inductor L_o via a switch S_1. The switch S_1 is the main switch, which allows the capacitor bank to discharge and has an assumed resistance of R_{S_1}. The capacitor bank is also equipped with a crowbar switch S_2, which is assumed to have a resistance R_{S_2}. The resistance and inductance of the rails are represented by the variable values R_{rail} and L_{rail} respectively. The variable value R represents the sum of the plasma-armature resistance with the resistance of the busbars and any possible stray resistance.

In the capacitively-driven stage, i.e. $t < t_c$, the Kirchhoff equation for the electric circuit in Figure 5 is:

$$\frac{Q}{C} + \frac{d}{dt}((L_o + L_{rail})I) + I(R_{S_1} + R_{rail} + R) = 0 \qquad (2)$$

where Q represents the charge on the capacitor bank for any time t before t_c and I equals dQ/dt.

In the inductively-driven stage, i.e. $t > t_c$, the Kirchhoff equation for the electric circuit in Figure 5 becomes:

$$\frac{d}{dt}((L_o + L_{rail})I) + (R + R_{S_2} + R_{rail})I = 0 \qquad (3)$$

In this report it is assumed that the inductance of the rails can be written in the following form:

$$L_{rail} = L'x(t) \qquad (4)$$

where L' is the inductance per unit length of the rails and x(t) is the displacement of the projectile. It is also assumed that the resistance of the rails can be written as:

$$R_{rail} = R'x(t) \qquad (5)$$

where R' is now the resistance of the rails per unit length. For the purposes of simplicity, it is assumed that both R' and L' are constant.

The current is determined as a function of time by solving Equations (2) and (3) for the two different stages. However, in their present forms both equations cannot be solved, so they must be simplified. In Subsection 5.5 it is seen that the projectile has travelled less than 5 cm in the first 200 μs for all firings in the RPIP series. By this time crowbarring of the capacitor bank has occurred. Thus the terms involving the displacement x(t) in Equation (2) can be neglected since both L' (approximately 0.40 μH/m) and R' (about 1.6×10^{-4} Ω/m) are also small. Assuming at this stage for convenience that the resistances R_{S_1} and R are constant and using the fact that the current is zero at t = 0, the solution to Equation (2) is:

$$I = I_m \exp(-R_{tot}t/2L_o)\sin((1/L_oC - R_{tot}^2/4L_o^2)^{1/2}t) \tag{6}$$

where $R_{tot} = R_{S_1} + R$ and $t < t_c$. A value for I_m is found by determining the value of the railgun current at a particular time. If $R_{tot}/2L_o << 1/(L_oC)^{1/2}$, then Equation (6) becomes:

$$I = I_m \exp(-R_{tot}t/2L_o)\sin((L_oC)^{-1/2}t) \tag{7}$$

and for the case where $R_{tot}t/2L_o << 1$, Equation (7) simplifies to:

$$I = I_m \sin((L_oC)^{-1/2}t) \tag{8}$$

The time at which the maximum value of current occurs is found by differentiating Equation (6) with respect to time and setting the result equal to zero. The following equation is obtained:

$$t_{max} = \frac{\pi}{2\omega} - \frac{1}{\omega}\arctan\left(\frac{R_{tot}}{2L_o\omega}\right) \tag{9}$$

where

$$\omega = (1/L_oC - R_{tot}^2/4L_o^2)^{1/2} \tag{10}$$

If $R_{tot}/2L_o << (1/L_oC)^{1/2}$, then Equation (9) can be simplified even further to become:

$$t_{max} \sim \frac{\pi}{2\omega}\left(1 - \frac{R_{tot}}{\pi L_o\omega}\right) \tag{11}$$

which indicates that t_{max} approaches $\pi/2\omega$ when $R_{tot}/L_o\omega$ approaches zero.

Another form of Equation (9) is:

$$\frac{1}{\omega} \arctan\left(\frac{R_{tot}}{2L_o\omega}\right) = \frac{\pi}{2\omega} - t_{max} \tag{12}$$

Since the left hand side of Equation (12) is positive, the following inequality is obtained:

$$\omega < \frac{\pi}{2t_{max}} \tag{13}$$

Squaring both sides of Equation (13) and using Equation (10) yields:

$$R_{tot} > 2L_o(1/L_oC - \pi^2/4t_{max}^2)^{1/2} \tag{14}$$

Using the values for L_o and C given in Section 4, $1/L_oC$ is found to be $(9.9 \pm 0.6) \times 10^7$ rad^2/s^2. In RPIP02, t_{max} was found to be 159 ± 5 μs and hence, $\pi^2/4t_{max}^2$ for this firing was equal to $(9.8 \pm 0.7) \times 10^7$ rad^2/s^2. Although using values of 9.9×10^7 for $1/L_oC$ and 9.8×10^7 for $\pi^2/4t_{max}^2$ yields a minimum value of 13 mΩ for R_{tot}, this value is not accurate because small differences in the various quantities in Equation (14) can produce significantly different values for R_{tot}.

If $R_{tot} \ll 2L_o\omega$, then t_{max} is approximately equal to $\pi/2\omega$. Denoting the peak current reached in a railgun firing as I_p, Equation (7) yields:

$$I_p = I_m \exp(-R_{tot}\,\pi/4\omega L_o) \tag{15}$$

Hence, Equation (7) in terms of I_p becomes:

$$I = I_p \exp(-R_{tot}(t - \pi/2\omega)/2L_o) \sin(\omega t) \tag{16}$$

where ω equals $(L_oC)^{-1/2}$.

If $R_{tot}(t - \pi/2\omega)/2L_o \ll 1$, then Equation (16) becomes:

$$\omega t \sim \arcsin(I/I_p) \tag{17}$$

Thus a plot of $\arcsin(I/I_p)$ against t yields a straight line with the gradient equal to the angular resonant frequency provided $R_{tot}(t - \pi/2\omega) \ll 2L_o$. This atter condition occurs when $t \sim \pi/2\omega$ and/or if $R_{tot} \ll 2L_o$.

A plot of $\arcsin(I/I_p)$ against time t for RPIP02 is shown in Figure 6. The points in this graph have been found by evaluating $\arcsin(I/I_p)$ directly from the experimental data taken at 10 μs time intervals between t = 0 and t = t_c (190 μs). The essential feature of the graph in Figure 6 is that $\arcsin(I/I_p)$ increases linearly between t = 0 and t = 160 μs with the gradient of the line equal to (9.9 ± 0.2) x 10^3 rad/s, which is almost equal to ω or $(L_oC)^{-1/2}$. Thus resistive damping caused by the factor $\exp(-R_{tot}t/L_o)$ appearing in Equation (7) is almost negligible for the first 160 μs of a RAPID railgun firing. It should be noted that when I approaches the peak value I_p in the vicinity of t ~ 160 μs, the values for $\arcsin(I/I_p)$ are subject to large variation for small deviations in the current.

Since the current in a RAPID railgun is given by Equation (8) with I_m equal to I_p, the energy in the storage inductor at peak current, which is given by $L_oI_p^2/2$, should be close to the energy initially stored by the capacitor bank $(CV_o^2/2)$ provided not much energy has been lost in the plasma-generation process. The energy in the storage inductor at peak current is found to be (2.1 ± 0.6) x 10^4 J, where a value of 81 ± 9 kA has been used for the peak current I_p. The value for I_p has been found by using the calibration factor of 92 ± 10 kA/V quoted in Reference [6] for current-time records. The large uncertainty in the calibration factor is mainly responsible for the large uncertainty in the energy in the storage inductor at peak current.

As the energy stored initially in the capacitor bank was 28.7 ± 0.6 kJ, there is a difference of approximately 6.7 ± 1.2 kJ between the energy stored by the capacitor bank initially and the energy in the storage inductor at peak current. Since the current-time behaviour is given by Equation (8), which implies that resistive energy losses during the capacitively-driven stage can be neglected, and the capacitors comprising the capacitor bank were not leaky, the large energy difference can only be accounted for as energy lost in plasma-generation. However, the energy difference could be smaller because the calibration factor of 92 kA/V is questionable and a higher value perhaps closer to 102 kA/V should be used when determining values for the railgun current.

In the inductively-driven stage the current is determined as a function of time by solving the following equation:

$$\frac{d}{dt}((L_o + L'x)I) + I(R + R_{S_2} + R'x) = 0 \qquad (18)$$

where Equations (4) and (5) have been used. Even if it is assumed that R and R_{S_2} are constant, Equation (18) can only be solved for the special case where $^2L_o/(R + R_{S_2})$ is to L'/R'. This case is discussed in the Appendix but, unfortunately, is not applicable to the RAPID railgun. Thus Equation (18) must be solved in asymptotic limits.

There are two asymptotic limits in which a knowledge of the displacement x(t) is not required for solving Equation (18). In the first asymptotic limit, $R'x \ll R + R_{S_2}$ and $L'x \ll L_o$. Equation (18) then simplifies to:

$$\frac{d}{dt}(L_o I) + (R + R_{S_2})I = 0 \qquad (19)$$

The solution to Equation (19), still assuming that R and R_{S_2} are constant, is:

$$I = I_o e^{-(R + R_{S_2})t/L_o} \qquad (20)$$

where I_o is the value of the current at t = 0. Since t = 0 in the inductively-driven stage corresponds to $t = t_c$ in a railgun firing, I_o in Equation (20) is the value of the railgun current at the instant when crowbarring of the capacitor bank occurred.

In the second asymptotic limit, $R'x >> R + R_{S_2}$ and $L'x >> L_o$. The solution to Equation (18) in this limit is:

$$I = I_d \exp(- R't/L')/x \qquad (21)$$

where I_d is the value for the product of the current and projectile displacement at the instant when the second asymptotic limit becomes valid. Since the RAPID railgun is 0.5 m in length and L' is expected to range from 0.32 μH/m to 0.54 μH/m [10], the maximum value of L'x is 0.27 μH. This value is considerably less than the inductance of the storage inductor used in the RPIP series. Hence Equation (21) does not need to be considered in the current-time analysis for the inductively-driven stage of a RAPID railgun.

To see whether Equation (20) is valid for part, if not all, of the inductively-driven stage, the parameter I/I_o has been plotted against time on a log-linear scale in Figure 7 using the current-time data for RPIP02. The value for I_o was chosen to be the value of the railgun current at t = 200 μs because this value was close to the value at $t = t_c$. As can be seen from Figure 7, the value of $\log_{10}(I/I_o)$ decreases linearly till about 500 μs after shot-start. Therefore Equation (20) is valid for describing the railgun current in this time-interval. Hence $(R + R_{S_2})/L_o$ can be regarded as being constant in this time interval. For times greater than 550 μs, the value of $\log_{10}(I/I_o)$ falls away from the straight line in Figure 7, thereby indicating that $(R + R_{S_2})/L_o$ is increasing.

For $(R_{S_2} + R)/L_o$ to increase, either $R_{S_2} + R$ must increase or L_o must decrease. In Equation (19), L_o represents the total inductance of the railgun circuit other than the inductance of the rails. Thus L_o includes the inductance of the storage inductor, the stray inductance of the busbars and the inductance of the plasma armature. The plasma inductance has been shown to be a negligible quantity [11] and the value of the stray inductances of the busbars is small in comparison with the inductance of the storage inductor. Hence, L_o approximately equals the storage inductance, which remains constant over the duration of the firing and thus $(R_{S_2} + R)$ must increase when $(R_{S_2} + R)/L_o$ increases.

The total resistance $(R_{S_2} + R)$ is composed of the resistance of the crowbar switch S_2, the plasma armature's resistance and the resistance of the

busbars, which is assumed to be constant. Thus when the total resistance increases in the inductively-driven stage, the plasma armature resistance and/or the resistance of switch S_2 must increase.

To see the increase in circuit resistance for times greater than 550 μs more clearly, a graph of the plasma armature impedance against time is shown in Figure 8 for RPIP02. The plasma armature impedance has been obtained by subtracting the electrode potential drops, which total at most 15 V [12], from the muzzle voltage and then dividing the resulting plasma potential difference by the current I at the corresponding time. Since the effect of the plasma armature's inductance is small [11], the plasma armature impedance becomes the plasma armature resistance as indicated in Figure 8.

It can be seen in Figure 8 that the plasma armature resistance stabilises after 0.3 ms, which is approximately 0.17 ms after shot-start. The plasma resistance is almost constant till about 0.55 ms as shown in Figure 8. Then the resistance begins to rise almost linearly with time until shot-out.

The time constant for the part of the inductively-driven stage when the RAPID railgun behaves as an LR circuit is obtained by evaluating the gradient of the line in Figure 7. If k is the gradient and τ is the time constant, then

$$\tau = \frac{-\log_{10} e}{k} \tag{22}$$

which yields a value of 8.3×10^{-4} s for τ in RPIP02. It should be noted that the time constant determined in this graphical manner is subject to an error of at least 10 percent. Since τ equals $L_o/(R_{S_2} + R)$, the total resistance in the railgun circuit during this part of the inductively-driven stage is 7.6 ± 1.2 mΩ.

The deviation of the current from the straight line in Figure 7 has already been attributed to a monotonic increase in the resistance of the railgun circuit. Much of this increase is due to an increase in plasma armature resistance occurring late in a firing as shown in Figure 8. If the increase in the total resistance can be regarded as being approximately linear in time, then Kirchhoff's law for the late part of the inductively-driven stage should be modified to become:

$$-L_o \frac{dI}{dt} = (R_{S_2} + R + \dot{R}\, t)I \tag{23}$$

where $\dot{R}$ represents the increase in the total resistance per unit time. Assuming $\dot{R}$ is constant, the solution to Equation (23) is:

$$I = I_2\, e^{-((R_{S_2} + R)t/L_o + \dot{R}\, t^2/2L_o)} \tag{24}$$

In Equation (24), t is measured from the onset of $\dot{R}$, which for RPIP02 was about 0.5 ms after plasma initiation and I_2 is the value of the railgun current at this time. Equation (24) serves to indicate that the time dependence in the expression for the railgun current becomes more complicated than is suggested by Equation (20). However, Equation (19) is also a simplification of the general Kirchhoff equation (Equation (3)) because it does not contain a dependence on the projectile displacement x(t). In view of the complex behaviour of the current, it is perhaps surprising that the railgun current is given by Equation (20) in the early part of the inductively-driven stage although a more detailed investigation by expanding the time and current scales in Figure 7 might yield a different result.

From Figure 5, it can be seen that in the capacitively-driven stage the main discharge switch S_1 is active while the crowbar switch S_2 remains inactive. In the inductively-driven stage the reverse applies. Since the switches are produced by exploding the same type of wire and hence are similar, it is expected that their resistances should be nearly equal. If it is assumed that the resistance of the capacitor bank is negligible because the small resistances of the capacitors are in parallel, then the resistance for the early part of the inductively-driven stage is approximately the same value as the total resistance in the capacitively-driven stage. Thus the time constant τ is about the same value as L_o/R_{tot} in Equation (6).

The energy dissipated due to resistive heating is obtained by integrating I^2R_{tot} with respect to time between t = 0 and the time at which peak current occurs. This energy, denoted by E_R, is given by:

$$E_R \simeq \int_o^{\pi/2\omega} I_p^2 \; R_{tot} \exp\left(-R_{tot}(t - \pi/2\omega)/L_o\right) \sin^2(\omega t)dt \qquad (25)$$

where $R_{tot} = L_o/\tau$ and Equation (16) has been used for the current. Integrating the right hand side of Equation (25) gives:

$$E_R \simeq \frac{I_p^2 R_{tot}}{2}\left[\frac{L_o}{R_{tot}}\left(\exp(\pi R_{tot}/2\omega L_o)-1\right) - \frac{R_{tot}}{L_o(R_{tot}^2/L_o^2 + 4\omega^2)}\left(1+\exp(\pi R_{tot}/2\omega L_o)\right)\right] \qquad (26)$$

After substituting the various physical parameters for RPIP02 into Equation (26) and assuming that the peak current was 81 kA, the total energy dissipated due to resistive heating is found to be (4.2 ± 0.4) kJ. The error in this result arises primarily from the first term on the right hand side of Equation (26).

An energy discrepancy of about 3.5 kJ still needs to be explained. Some energy is lost in the creation of the plasma armature, which is estimated as follows. In RPIP02, a piece of aluminium foil of mass 0.017 g was used to create the plasma. This mass corresponds to 3.8×10^{20} aluminium atoms. If

it takes about 10 eV on average to ionise each aluminium atom so that a plasma containing a mixture of first and second ionised ions is formed, then the energy required to create the plasma would be approximately 0.6 kJ. However, this approach does not account for the 3.5 kJ discrepancy noted above. It is probable that 0.6 kJ is an under-estimate since additional explosive effects could be present and/or the calibration factor used for the current records might be higher. Another and more recent calibration of the current-time records suggests that the factor of 92 kA/V was indeed too low [13].

The current-time records of the other RPIP firings were analysed in the same manner as the current-time record for RPIP02. The results for the angular resonant frequencies, time constants and circuit resistances appear in Table 3. The slight variation in the values for the angular resonant frequencies is attributed to differences arising in the plotting of the current-time records. In stating the values for the time constant, an error of typically 10 percent is likely. The errors for the angular frequency and time constant were used to evaluate the errors for the external inductance and circuit resistance for each firing listed in Table 3. Although the values of the external inductance and circuit resistance vary, most of the variation is accounted for by the errors or uncertainties. Thus the effect which different foil types and masses had on the time constant and circuit resistance was not significant.

It was found that the resistance of the plasma armature began to increase about 0.5 ms after shot-start for those firings in which no arcing occurred ahead of the projectile. However, unlike the result shown in Figure 8, the resistance of the plasma armature did not increase linearly in most of the firings. The firings in which the plasma resistance increased almost linearly with time were RPIP04, RPIP06 and RPIP22. As mentioned previously, these firings were among the more successful firings in the RPIP series.

5.3 Streak Photographs

A copy of streak photograph for RPIP02 is shown in Figure 9. In this figure the streak represents the motion of the plasma armature during acceleration. The width of the streak represents the length of the major current-carrying portion of the plasma armature while the displacement of the plasma armature is measured horizontally to the right. If the leading edge of the streak is distinct, then the amount of plasma leakage is insignificant. Since the amount of plasma leakage was not significant in RPIP02, the leading edge of the streak is assumed to correspond to the back of the projectile. The total displacement of the projectile was 448 mm, which means that each mm of the actual streak photograph in the horizontal direction corresponds to 16.7 ± 0.7 mm of gun-body length. In addition, if the total duration of the firing is given by t_f, then

$$t_f = (f_T l_v)/M \qquad (27)$$

where f_T is the time factor for the camera (17.73 μs/mm for RPIP02), l_v is the total vertical length of the actual streak (about 195 mm for RPIP02) and M is

the magnification factor (4.48 for RPIP02). The total duration of RPIP02 was $(7.7 \pm 0.2) \times 10^2$ μs, which means that each mm of the streak photograph in the vertical direction corresponds to 4.0 μs. It should be noted that the horizontal and vertical scales of the streak photographs mentioned hereafter in this report pertain to the actual streak photographs obtained during the RPIP series and not to the reduced images shown in the various figures in this report.

The frame record for RPIP02 is shown in Figure 10. In this figure the position of the plasma armature is shown at intervals of about 50 μs . Narrow beams of light in front of and behind the plasma armature are also indicated.

Although the frame record for RPIP02 indicates that some plasma leakage occurred during acceleration, this loss was not considered to be substantial because it was not conspicuous on the streak photograph for RPIP02. As mentioned previously, the streak camera accepted a narrower range of light and hence would not have recorded as much detail as the frame camera. However, a close inspection of the leading edge in Figure 9 does reveal a fuzziness which is an indication that plasma is leaking ahead of the projectile.

RPIP02 has been described as one of the most successful firings in the series because, in addition to there being little plasma-leakage, there was no arcing ahead of the projectile and no plasma breakup or disruption occurring during acceleration. Examples of firings in which the above effects appear are RPIP01, RPIP15 and RPIP19, whose streak photographs appear in Figures 11, 12 and 13, respectively.

Both plasma breakup and leakage appear in the streak photograph for RPIP01 as shown in Figure 11. The plasma breakup or disruption, which is represented by the separation occurring within the plasma armature, appears short-lived. This is perhaps an indication that when this effect occurs in a RAPID railgun, the plasma armature is able to re-stabilise itself. The leakage of plasma ahead of the projectile did not result in arcing occurring ahead of the projectile. However, plasma leakage caused an early activation of the fibre-optic probe which was situated close to the muzzle. Thus it was difficult to pinpoint exactly when the projectile had passed directly under the probe on the time-of-arrival record. This led to the dubious result for the velocity appearing in the first row of the second column of Table 2.

A more severe example of plasma disruption is shown in Figure 12. Each mm in the vertical direction of the streak photograph corresponds to about 4.0 μs of actual time while each mm in the horizontal direction corresponds to an actual length of about 17 mm. The region of greatest plasma disruption occurred between $t \approx 0.2$ ms and $t \approx 0.4$ ms as shown in the figure. When plasma breakup or disruption occurs, a dark region appears inside the streak, which indicates separation of the plasma. At the edges of the separation large density or temperature gradients result. It is interesting to note that in Figure 12 the separation within the plasma has completed one oscillation by moving from the rear of the plasma to its front and then returning to the rear of the plasma before re-stabilisation occurs.

An example of arcing ahead of the projectile is shown in Figure 13. An interesting feature of this figure is that, as the runaway arc increased its length during the firing, the length of the plasma armature decreased. However, once the runaway arc had been ejected, the length of the plasma armature increased suddenly. This behaviour is discussed in more detail in Section 7.

The three phenomena described in this section all indicate that the plasma armature in an electromagnetic launcher might not be as stable and uniform in density as previously thought. In the plasma model for the PARA code [2], it is assumed that the mass of the plasma is constant during acceleration. This can only be true if the mass of plasma leaked is replaced exactly by an equivalent mass of material ablating off the rails and gun-body, which is unlikely as is discussed in the section on rail damage. If the mass of plasma leaked is insignificant, as in RPIP02, then the constant plasma mass limit of the PARA code is approached provided the ablation of material into the plasma armature is also negligible.

In the PARA code it is assumed that at any given instant the electron density and internal temperature are uniform over the length of the plasma armature. However, when plasma disruption occurs, the electron density and internal temperature are no longer uniform over the plasma length. Thus the PARA code is not applicable to those firings in which plasma disruption occurs over a long time interval with respect to the total duration of a firing, e.g. RPIP15.

Plasma leakage occurred in the RPIP series because the RAPID railguns had been used extensively before the RPIP series. The gun-bodies were reversed after RPIP20 because it was believed that obturation would be better. Although reversing the gun-bodies was able to stop arcing occurring ahead of the projectile in a few firings after RPIP20, plasma leakage did not cease.

Plasma leakage and arcing ahead of the projectile can be attributed to an inability of the magnetic field acting within the plasma armature to confine the plasma armature completely. It is also very probable that the magnetic field might be indirectly responsible for the production of the large density or temperature gradients within the plasma when plasma disruption occurs. Thus determination of the magnetic field acting within the plasma is important in gaining an understanding of the stability of plasma armatures in electromagnetic launchers.

From Table 1, it can be seen that plasma breakup was most likely to occur in firings involving larger masses of plasma initiating foil. This suggests that in larger railguns where heavier pieces of metallic foil could be required to generate the plasma, there might be a greater tendency for this type of plasma instability to occur. Therefore, before larger designs of railguns can be considered, it may be necessary to undertake a stability analysis of the plasma armature.

5.4 Muzzle Voltage Records

The muzzle voltage records for RPIP02, RPIP15 and RPIP19 are shown in Figures 14, 15 and 16 respectively. These figures show that a plateau region develops after a period of time lasting in some cases up to a couple of hundred microseconds. In many cases the muzzle voltage in the plateau region is almost constant or decreases marginally as can be seen in Figure 14 from t = 0.3 ms onwards. Noisiness in the plateau region, which begins about 0.15 ms from shot-start is believed to correspond with the occurrence of plasma leakage. When severe plasma breakup occurs as was shown in the streak photograph for RPIP15 (Figure 12), the plateau region fluctuates significantly. In RPIP15 this occured between 0.2 and 0.4 ms from shot-start. When a runaway arc appears as in RPIP19, the muzzle voltage record displays a sudden peak corresponding to the ejection of the runaway arc. After the runaway arc's exit, which occurs about 0.38 ms from shot-start in Figure 16, the muzzle voltage reverts to its previous value. At the end of the plateau region there is another abrupt peak in the muzzle voltage record which corresponds to the plasma armature's exit. This peak occurs approximately 1.1 ms from shot-start and hence can be used to determine the total duration of a firing. It should be noted that the sudden peaks and fluctuations appearing on the muzzle voltage records also appear on the breech voltage records.

An interesting feature in Figures 14 to 16 is the reversal in polarity of the muzzle voltage after ejection of the plasma armature. The most likely explanation for this behaviour is that the transient recorder connected to the muzzle measures the voltage across the crowbar switch. This switch could still be conducting current supplied by the capacitor bank provided the main switch is able to conduct current.

The most interesting feature about the muzzle voltage records was that the muzzle voltage was nearly constant when there was no plasma breakup and arcing ahead of the projectile. Once the plasma armature had settled into the plateau region, the muzzle voltage varied slowly with time, decreasing from about 190 to 150 V. Since the current was decreasing exponentially in the inductively-driven stage, the resistance of the plasma armature increased as shown in Figure 8.

The resistance of the plasma armature is given by:

$$R_a = \frac{\eta_a w}{l_a h} \qquad (28)$$

where w is the width of the railgun bore, h is the height of the bore and l_a is the length of the plasma. In Equation (28), η_a is the average plasma resistivity, which according to the Spitzer formula [14] depends on the average internal temperature (T), the average electron density (n_e) and the degree of ionisation (α). Since the width and height of the bore are constant, an increase in plasma armature resistance means that the ratio of η_a/l_a must increase. The resistivity of the plasma armature increases generally when the plasma temperature decreases. A temperature decrease occurs when the amount of ohmic heating decreases, and this in turn is caused by decreasing current. Thus the plasma length does not need to decrease for the plasma resistance to increase.

One of the aims of the RPIP series was to observe if there was an effect on the muzzle voltage records due to different foil masses and types. The differences appearing in the muzzle voltage records have already been attributed to other factors and therefore it was difficult to attribute any strange behaviour on the records to a foil type and mass. In the early stage of a firing the foil mass and type are expected to have their greatest effect on the muzzle voltage records because the plasma armature is believed to be composed mainly of the material in the foil at this time. However, although the current rise-time behaviour varied on the records, it was not possible to attribute differences to a specific type and mass of metallic foil.

5.5 Position-Time Results

Projectile displacement-time results could not be obtained for RPIP23 to RPIP25 because the streak films for these experiments were either not recorded or were poorly developed. In firings with arcing ahead of the projectile such as RPIP08, RPIP10 and RPIP17 to RPIP20, the projectile's point of exit could not be pinpointed on the streak photograph because the streak faded towards the end of these firings as can be seen in Figure 13. Thus the streak photographs for these experiments could not be analysed properly. Although the streak photographs for RPIP21 and RPIP24 did not show arcing ahead of the projectile, projectile displacement-time data were not obtained because the point of exit could not be established. Only 14 streak photographs were suitable for obtaining displacement-time data.

Another problem in obtaining displacement-time data was that the $t = 0$ point or the origin could not be established easily because the onset of the streak did not necessarily mean that the projectile had been set in motion. Furthermore, it was assumed that the leading edge of the streak corresponded to the position of the back of the projectile. Because of these uncertainties the displacement-time data are subject to an error of at least 10 mm for the projectile's position and at least 10 μs for the time. Thus the errors in the projectile's position and time are significant initially but towards the end of a firing when the displacement is about 450 mm and the time is above 750 μs, the errors become relatively smaller.

The projectile's position as a function of time during acceleration for RPIP02 is shown in Figure 17. In this figure the projectile's position is given by the dots on the graph. Although difficult to distinguish, curve fits of the displacement in the form of quadratic and cubic polynomials in time also appear in Figure 17. As expected, both curves deviate from the experimental results in the early stage of motion where the displacement is relatively inaccurate. For displacements greater than 80 mm, which correspond to the inductively-driven stage, both curves are in excellent agreement with the experimental results. This would indicate that within experimental error either a cubic or quadratic polynomial in time can be used to represent the displacement of the projectile in RPIP02. In fact this behaviour was found to apply to all of the RPIP firings analysed in this section.

The values for the coefficients of the quadratic and cubic curve fits for fourteen RPIP experiments appear in Table 4. Accompanying these values are the uncertainties as estimated by GRAPH [7]. As a result of these

uncertainties, many different curves can fit the experimental data adequately. The correlation coefficient (p) is an indication of the accuracy of the least squares method used to determine the coefficients of the polynomials and should be close to unity for accurate curve fits.

Even though both the quadratic and cubic displacement time curves can be used to represent the displacement of the projectile, these curves yield different acceleration predictions. If the displacement of the projectile is described by a quadratic function in time, then the acceleration is constant. On the other hand, if the displacement is described by a cubic function in time, then the acceleration is a linear function in time. For the two curves to yield similar results it must be shown that the cubic term represents only a small correction to the quadratic displacement-time curve. Therefore if the quadratic displacement-time curve given by

$$x(t) = at^2 + bt + c \tag{29}$$

and the cubic displacement-time curve given by

$$x(t) = a_1t^3 + b_1t^2 + c_1t + d_1 \tag{30}$$

are to yield similar results, then according to Reference [15], it is necessary that $a_1t^3 \ll b_1t^2 + c_1t + d_1$ and that b_1, c_1 and d_1 must closely equal a, b and c respectively.

From Table 4, it can be seen that the contribution a_1t^3 is small early in a firing but becomes large late in a firing. Allowing for the uncertainties, the coefficients of the quadratic curve are different from the other coefficients of the cubic curve and hence it is difficult to decide which, if any, of the curves should be used to describe railgun perfromance. Nevertheless, it is useful to obtain estimates for the velocity of the projectile by differentiating the curves in Table 4 with respect to time for times greater than 0.16 ms. Differentiating the curves twice with respect to time yields estimates for the acceleration. In each firing listed in Table 4, the coefficients of the cubic and quadratic terms of the cubic polynomial are negative and positive respectively, thereby indicating a linear acceleration with negative gradient. Therefore the acceleration is decreasing with increasing time but because the acceleration remains positive, the velocity of the projectile continues to increase. This behaviour is expected in a railgun firing and is explained in the following paragraphs. It should be noted, however, that the average accelerations obtained from the cubic curves agree closely with the accelerations obtained from the corresponding quadratic curves.

The equation of motion for the plasma-projectile system in a railgun is:

$$(m_a + m_p)\frac{dv}{dt} = \frac{1}{2}L'_pI^2 - f \tag{31}$$

where m_a and m_p are the masses of the plasma armature and projectile respectively and f is a general retarding term which includes friction and atmospheric effects [16] acting against the plasma-projectile system. In Equation (31), m_a and m_p are assumed constant and L_p' is the propelling inductance, which is given by:

$$L_p' = \frac{\int_{U_a} 2|\underline{j} \times \underline{B}| \, dU}{I^2} \tag{32}$$

In Equation (32), $\underline{j}$ and $\underline{B}$ are respectively the current density and magnetic field in the plasma armature while U_a is the volume of the plasma armature. The propelling inductance per unit length is not necessarily equal to the more commonly-used rail inductance per unit length L'. However as a simplification, when quoting values for L_p' in this report, values for L' are used.

Because the current in the RAPID railgun decreases after 0.16 ms, and retardational effects are usually considered to become greater as the velocity increases, Equation (31) indicates that the acceleration of the plasma-projectile system must decrease. This is the type of behaviour exhibited by the cubic displacement-time curves given in Table 4. However, this behaviour is not unique to cubic displacement-time curves because higher order polynomials in time can exhibit the same behaviour.

In actual fact, it might be necessary to consider higher order polynomial fits especially early in a firing. When the time t is close to zero, the factor $\exp(-R_{tot}t/2L_{tot})\sin(\omega t)$ becomes approximately equal to ωt. Thus, for $t \simeq 0$, Equation (31) becomes:

$$(m_a + m_p)\frac{d^2x}{dt^2} \simeq \frac{1}{2} L_p' I_m^2 \omega^2 t^2 \tag{33}$$

where the retarding force term has been assumed to be negligible because the velocity is small initially. The solution to Equation (33) is a quartic polynomial in time.

5.6 Velocity Data

The graph of velocity versus time for RPIP02 is shown in Figure 18. The values for the projectile velocity were obtained by calculating central differences for the experimental displacement-time data of RPIP02. Values were chosen at time intervals of 40-70 μs so that a reasonably accurate velocity-time analysis could be carried out. Subtracting projectile position results between smaller time intervals would lead to highly inaccurate results for the velocity whereas subtracting the position results between larger time intervals would produce velocities which could no longer be regarded as instantaneous.

The velocity values are unreliable early in a firing because of the greater relative errors in the projectile's position and time. Some of the

velocities appearing in Figure 18 have errors up to ± 300 m/s and hence the graph serves mainly as a guide. This discussion demonstrates that an alternative technique for determining the instantaneous velocity of the projectile during a railgun firing is required, particularly early in a railgun firing.

An interesting feature of the graph in Figure 18 is its linearity between 350 and 750 μs, which suggests that the acceleration can be regarded as being constant in this time interval. The gradient of the line of best fit through the points in this time interval yields a value of 10.5×10^5 m/s^2 for the acceleration. This value compares favourably with twice the value given in Table 4 for the leading coefficient of the RPIP02 quadratic displacement-time curve. Thus the first and second time derivatives of the displacement-time curves in Table 4 appear to yield reasonable estimates for the velocity and acceleration of the projectile except early in a railgun firing.

The values for the projectile's exit velocity obtained from the quadratic and cubic displacement-time curves for RPIP02 are 1.02 and 0.97 km/s respectively. To obtain these values, an exit time of 780 μs has been taken from the data for RPIP02 and the uncertainties in the coefficients have been neglected. Extrapolating the linear portion of Figure 18 yields an exit velocity close to 1.0 km/s, which is greater than the value of 923 m/s for the RPIP02 muzzle flash-to-laser beam velocity listed in the second column of Table 2. Therefore an exit velocity of 1.0 km/s is probably incorrect. The uncertainties in the coefficients of the quadratic displacement-time curve only reduce the estimated exit velocity to 1.0 km/s. Thus exit velocities obtained from the cubic displacement-time curves are more likely to agree with the experimental results in Table 2 later in a firing.

5.7 Plasma Length Measurements

Plasma-armature lengths were obtained for many of the RPIP firings by using the light-intensity profiles at various points along the streak film. Three examples of plasma intensity profiles taken from RPIP02 appear in Figures 19, 20 and 21. Figure 19 shows the light intensity profile of the plasma armature when its leading edge was situated about 1.1×10^2 mm from the initial position or approximately 2.2×10^2 μs after shot-start. The plasma's initial position is assumed to be 47 mm from the closed breech because this was where the rear of the projectile was situated at shot-start. The leading edge of the plasma armature in Figure 20 is about 40 mm from the initial position. Figure 20 shows the plasma intensity profile when $t \approx 3.4 \times 10^2$ μs after shot-start. The position and time of the leading edge of the plasma in Figure 21 was not recorded but it is believed that the figure shows the plasma between the times and positions given for Figures 19 and 20.

As can be seen from Figures 19 to 21, the plasma armature is characterised by abrupt changes in light intensity at its front and rear edges. The maximum light intensity in Figure 19 is a factor of about 64 times the background intensity level whilst the maximum light intensity levels in Figures 20 and 21 are about 44 and 90 times the background level respectively. These intensity factors have been determined approximately by using a logarithmic scale with the background light-intensity level set to unity.

The distance over which the sharp rise in light intensity is raised in Figures 19 to 21 is used as a measure of the plasma armature's length. In order to be consistent, plasma length measurements were made at the same light intensity level relative to the background intensity level throughout each firing. Although this standard light intensity level varied sometimes from one firing to another, comparisons of the measurements obtained in a particular firing could be made with each other. Thus the plasma lengths in Figures 19, 20 and 21 were found to be about 40, 42 and 57 mm respectively at an intensity level about three times the background intensity level. The plasma length value obtained from Figure 21 may, however, not be a true indication of the plasma length as is explained later in this section.

The three figures show that the light intensity within the plasma armature is not always uniform. In particular, Figure 20 shows that during RPIP02 there were three distinct peaks present. The second peak in light intensity in Figure 20 is a distance of about 4 mm from the peak nearest the back of the plasma armature while the third peak is a further 15 mm away from the second intensity peak. The light intensity peaks appearing within the profile suggest that the internal temperature and density of the plasma armature can vary substantially over its length. The appearance of temperature or density gradients suggest that the plasma armature might have a tendency to become unstable.

It is interesting to note that apparently no density or temperature variations were observed on the streak photograph for RPIP02 (Figure 9). As a result of this, the plasma armature was considered to be uniform in density and temperature throughout the entire firing. However, a closer inspection of the streak photograph indicated that some plasma leakage had occurred between 1.4×10^2 μs and 3.2×10^2 μs. In Figure 21, it can be seen that the leading edge of the plasma intensity profile has an additional hump for light-intensities below six times the background intensity level. Because the leading edge is no longer vertical at low light intensities, the additional hump has been produced by plasma leaking ahead of the projectile. Since the plasma length is measured between the leading and trailing edges of the profile at three times the background intensity level, the plasma length obtained from Figure 21 is not an accurate indication of the actual plasma length.

For most of the RPIP firings, the plasma length ranged between 3 and 15 mm for times close to plasma generation. For times greater than 200 μs, the plasma length generally ranged from 25 mm to 45 mm. The largest plasma armature length observed was about 94 mm, which occurred in RPIP13. However this length measurement included plasma leaking ahead of the projectile like that shown in Figure 21. A length of 71 mm was obtained for RPIP25 but this also included plasma leakage.

Figure 22 shows the formation of a runaway arc for RPIP26. In this figure much plasma has leaked ahead of the projectile and has been able to draw some of the railgun current away from the plasma armature. In general runaway arcs increased in length during firings and eventually became much larger than the plasma armature. Runaway arc lengths were able to reach lengths of over 100 mm.

The graphs of plasma length against time for RPIP01 and RPIP02 appear in Figure 23. The plasma lengths for RPIP01 were determined at a light intensity level of about three times the background level while the lengths for RPIP02 were determined at about twice the background level. In the case of RPIP01, the plasma armature lengths varied considerably, mainly due to the significant amount of plasma leakage occurring before 500 μs (see Figure 11). In the case of RPIP02, the plasma length appears to range between 25 and 40 mm except for the value at about 280 μs after shot-start. The length around 280 μs is the dubious plasma length obtained from Figure 21. The errors in the length values for both graphs in Figure 23 are about $\pm$ 4 mm while the time errors are about $\pm$ 50 μs. With so few points and such inaccuracy there is little justification for fitting curves to these graphs.

The results indicate that the maximum light intensity on the plasma intensity-profiles varies considerably even in a firing which has little plasma leakage, no arcing ahead of the projectile and no plasma disruption. However, in firings where the plasma armature is well-behaved, the plasma length and hence the plasma volume do not vary substantially.

The PARA railgun simulation code predicts that the length/volume of the plasma expands to a maximum value after the plasma has been generated because the "explosive" propulsion force (2) is initially greater than the Lorentz ($\underline{j} \times \underline{B}$) force. When the Lorentz force begins to dominate in a firing, the code predicts that the plasma contracts considerably reaching a minimum volume at peak current. As the current begins to decay in the inductively-driven stage, the internal gas pressure becomes more dominant. For low values of current, the plasma armature begins to expand appreciably, until at projectile exit the plasma volume is about five times the minimum value predicted at peak current.

It should also be noted that in the PARA code the plasma length is initially set equal to the distance between the rear of the projectile and the breech of the gun, i.e. 47 mm. At projectile exit the code predicts plasma lengths almost three to four times the initial length. The plasma length was seldom equal to or greater than 47 mm in the entire RPIP series. In addition, the continuous expansion of the plasma armature due to the exponential decay of the railgun current was not observed in the RPIP series. Therefore the PARA predictions for the plasma length/volume versus time do not agree with the actual plasma length behaviour observed in a RAPID railgun.

Since the plasma length was found to be relatively steady in a firing with a well-behaved plasma armature, e.g. RPIP02, it is suggested that the assumption of a constant plasma length/volume during acceleration might be a more appropriate way to model the plasma armature than assuming a constant plasma mass, which was employed in the PARA code.

5.8 Temperature Estimates for the Plasma Armature

In this section temperature estimates for the plasma armature are obtained by using three different methods. Firstly, it is assumed that the plasma armature behaves as a black-body with the energy loss due to radiative

flux equal to the energy due to ohmic heating of the plasma. Secondly, the results of the one-dimensional arc-dynamics code developed by Powell and Batteh [17, 18] are used in conjunction with the Spitzer expression for the electrical conductivity of a plasma [14]. The temperature estimates obtained from these two methods are then used as a check on the third method in which a computer code developed by Kovitya [19] is used.

If it is assumed that the plasma armature behaves as a black-body, then the heat flux at its surface is given by

$$Q_r = \sigma_s T^4 \tag{34}$$

where σ_s is Stefan's constant (5.67×10^{-8} $Jm^{-2}K^{-4}s^{-1}$). An estimate for the plasma temperature can be obtained by using the following equation

$$I\,(V_M - V_{el}) \simeq 2\,(wh + l_a h + l_a w)\,\sigma_s T^4 \tag{35}$$

where V_{el} is the total potential drop across the electrodes and is assumed to be about 15 V [12].

The approximate values for I, V_M and l_a at a time of 200 μs after shot-start in RPIP02 were found to be 77 ± 8 kA, 180 V and 38 mm respectively. Introducing these values into Equation (35) yields a plasma temperature of $(2.1 \pm 0.1) \times 10^4$ K. At shot-out the approximate values for I, V_M and l_a in RPIP02 were found to be 33 ± 4 kA, 150 V and 28 mm respectively. Using Equation (35) with these values yields a plasma temperature of $(1.7 \pm 0.1) \times 10^4$ K at shot-out.

The estimates for the plasma temperature using Equation (35) are expected to be higher than the actual average temperature because this method neglects other possible heat-loss mechanisms. Hence another method is now used to determine the plasma temperature.

If it is assumed that boundary effects between the plasma armature and the rails are negligible, then the muzzle voltage V_M becomes the sum of three distinct voltages. That is:

$$V_M = R_a I + V_{el} + L_p \frac{dI}{dt} \tag{36}$$

where R_a is the resistance of the plasma armature given by Equation (28) and L_p is the plasma inductance. The potential V_{el} is assumed to be about 15 V as before while the plasma inductance is considered to be negligible according to Reference [11]. Introducing Equation (28) into Equation (36) with the above simplification yields:

$$\eta_a \frac{wI}{l_a h} \simeq V_M - 15 \tag{37}$$

where the average plasma resistivity η_a is given by the Spitzer expression [14]:

$$\eta_a = \frac{Z}{2.63 \times 10^{-2}\ \gamma_E T^{3/2}} \log_e\left(\frac{1.23 \times 10^7\ T^{3/2}}{Z\ n_e^{1/2}}\right) \quad (38)$$

In Equation (38), T is the average temperature, n_e is the average electron density and γ_E is the ratio of the electrical conductivity of the plasma to that of a Lorentz gas. The parameter γ_E depends on Z, which in turn is given by:

$$Z = \frac{x_1 + 4x_2}{x_1 + 2x_2} \quad (39)$$

where x_1 and x_2 are the concentrations of first and second- ionised species respectively. Equation (38) is the expression used by Powell and Batteh in their one and two-dimensional arc-dynamics codes [17,18,20,21]. It should be noted that according to Ichimaru [22], the logarithmic term in Equation (38) is dependent on $Z^{-3/2}$ rather than Z^{-1}. Since values of Z close to unity are considered here, this discrepancy is neglected.

The logarithmic term in Equation (38) is now shown to be a slowly-varying quantity by using the predictions of the Powell and Batteh one-dimensional arc-dynamics code for two railgun plasma extremes. The version of this code available at MRL predicts that a plasma with an electron density of 3.9×10^{24} m^3 will have values of 0.82 and 0.04 respectively for the concentrations of first and second-ionised copper at a temperature of about 2.2×10^4 K. Under these conditions the value of the logarithmic term appearing in Equation (38) is about 3.0. The code also predicts that a plasma with an electron density of 6.5×10^{25} m^{-3} and a temperature of 5.98×10^4 K will have values of 0.0 and 1.0 for x_1 and x_2 respectively. For this case the value of the logarithmic term in Equation (38) becomes approximately equal to 2.4. Thus there is slight variation in the values of the logarithmic term in Equation (38) for the two plasma extremes.

Before a suitable value between 2.4 and 3.0 can be assigned to the logarithmic expression in Equation (38), it must be shown that the electron density n_e of a railgun plasma can reach the densities mentioned in the previous paragraph. Given that the mass of the aluminium foil used in RPIP02 was about 0.012 g and assuming that the foil on initiation was completely first-ionised, the number of electrons available in the plasma armature is about 2.7×10^{20}. As discussed in the last section, the plasma length was found to be about 35 ± 10 mm. Hence plasma volume is approximately $(1.7 \pm 0.5) \times 10^{-6}$ m^3 and the electron density is $(1.6 \pm 0.4) \times 10^{26}$ m^{-3}. Thus the electron density of a railgun plasma can reach levels where a value between 2.4 and 3.0 can be assigned to the logarithmic term appearing in Equation (38), provided the resultant temperature estimate for the plasma armature is of the order of 10^4 K.

The logarithmic term in Equation (38) is now set equal to a value of 3.0 because it is believed that the average plasma temperature is closer to 2.2×10^4 K rather than 5.9×10^4 K [23]. If it is also assumed that the plasma is first-ionised so that γ_E equals 0.5816 [24], then Equation (38) becomes:

$$\eta_a \sim \frac{2.0 \times 10^2\ Z}{T^{3/2}} \quad (40)$$

As mentioned previously, after the plasma had been generated, the muzzle voltage remained steady in those firings where no plasma instability and no arcing ahead of the projectile occurred. In such firings the muzzle voltage is approximately 180 V, which yields a value of 165 V for the right hand side of Equation (37). After the muzzle voltage had settled, the railgun current varied between 34 kA and 66 kA, where the uncertainty due to the current calibration factor has been taken into account. Therefore the resistance of the plasma armature varies between 2.5 and 4.6 mΩ, which agrees with Figure 8.

As stated in the previous section, it was found experimentally that the plasma length l_a ranged between 25 and 45 mm. From Equation (28), the resistivity of the plasma armature ρ_a equals 0.75 $R_a l_a$ for a RAPID railgun. According to Figures 8 and 23, the plasma length was slightly larger for lower values of the plasma-armature resistance. Thus setting R_a equal to 4.6 mΩ and l_a to 25 mm yields a value of 8.6×10^{-5} Ωm for ρ_a whereas setting R_a equal to 2.6 mΩ and l_a to 45 mm yields a value of 8.8×10^{-5} Ωm for ρ_a. Setting R_a equal to 2.6 mΩ and l_a to 25 mm yields a minimum value of 4.9×10^{-5} Ωm for ρ_a, which is used to determine an estimate for the maximum average temperature of the plasma armature.

For temperatures close to 2.0×10^4 K, the degree of second ionisation is small and the value of Z approaches unity. In one of the previously mentioned examples obtained from the Batteh and Powell code, Z was found to be equal to 1.1 when the temperature was equal to 2.2×10^4 K. If a value of 1.1 is introduced into Equation (40) for Z, then the average temperature of the plasma armature with the resistivity ρ_a set equal to 8.7×10^{-5} Ωm becomes 1.9×10^4 K. A value of 1.0 for Z with the same value for ρ_a yields an average plasma temperature of 1.7×10^4 K.

A maximum average temperature is obtained by setting ρ_a equal to 4.9×10^{-5} Ωm and using a slightly higher value for Z to account for the increase in the concentration of second ionisation x_2. At temperatures around 3.0×10^4 K, Z is approximately equal to 1.5. Using this value for Z in Equation (40) yields a maximum average temperature of 2.6×10^4 K. Thus the average internal temperature of the plasma armature is expected to be around 1.7×10^4 K with a maximum possible temperature close to 2.6×10^4 K. However, it is unlikely that the plasma temperature reaches 2.6×10^4 K because using the first method yielded a temperature of $(2.1 \pm 0.1) \times 10^4$ K.

The estimates for the plasma temperature obtained from the second method have relied on the validity of the Spitzer expression for the electrical conductivity. According to Cohen, Spitzer and McR. Routly [25], Equation (38) becomes less valid as the electron density increases above 10^{24} electrons/m^3 and the temperature decreases below 10^6 K. In order to verify the low temperature estimate obtained by using Equation (38), a computer code developed by Kovitya [19] was used. This code predicts many physical properties of partially and fully-ionised plasmas including the electrical conductivity and has been used by Kovitya and his co-workers in their studies of ablation-dominated arcs and sun-spot activity. They report good agreement with experiment in References [26-28]. Details concerning the applicability of this code to railgun plasmas have been reported elsewhere [29].

Before Kovitya's code can be used, the temperature and pressure ranges of interest need to be specified together with the mole fractions of the various neutral species initially comprising the plasma. In the successful firing RPIP06, a piece of copper foil was used to generate the plasma and thus it is assumed that the plasma was composed entirely of copper atoms and ions throughout the firing. That is the amount of cadmium, which comprised only 0.6% of the rails, and the amount of material ablated from the rails and RAPID gunbody, are assumed to be negligible. In addition, since plasma temperatures between 1.7×10^4 and 2.6×10^4 K have been obtained by using Equation (38), the range of temperatures to be considered when using Kovitya's code is from 0.8×10^4 to 2.6×10^4 K.

Estimates for the plasma pressure after the muzzle voltage had stabilised are obtained by using the following equation [30]:

$$p \simeq \frac{L' I^2}{2A} \qquad (41)$$

where L' has replaced L'_p and m_p is assumed to be much greater than m_a. Putting L' and I equal to maximum values of 0.54 μH and 66 kA, respectively, yields a pressure of about 2.4×10^7 Pa or 2.4×10^2 atm., whereas putting L' and I equal to minimum values of 0.32 μH and 34 kA yields a pressure of approximately 3.8×10^6 Pa or 0.4×10^2 atm.

The graphs of the electrical conductivity for a copper plasma at pressures of 2.4×10^2 and 0.4×10^2 atm. are shown in Figure 24. This figure shows that the plasma is more conductive at lower pressures for temperatures below approximately 1.6×10^4 K whereas for temperatures above 1.6×10^4 K, the plasma becomes more conductive at higher pressures.

Figure 25 shows the muzzle voltage record for RPIP06. After a period of about 0.35 ms, the muzzle voltage settled to a value close to 1.9×10^2 V for approximately 0.3 ms and then decreased steadily to a value close to 1.6×10^2 V at shot-out. Assuming that the total potential of the electrodes was 15 V [12], the potential difference across the plasma was therefore between 1.8×10^2 and 1.5×10^2 V.

Since the potential difference across the plasma was 1.8×10^2 V when the railgun current was 66 kA about 0.3 ms after shot-start, the plasma resistance was 2.7 mΩ. The microdensitometer reading at this instant of the firing showed no density or temperature variation over the plasma length. The plasma length was found to be 30 mm at a light-intensity of three times the background level. Using Equation (28) yields a value of 6.1×10^{-5} Ωm for the plasma resistivity and since electrical resistivity is the reciprocal of electrical conductivity, the electrical conductivity is found to be 1.6×10^4 S/m. According to Figure 24, this value corresponds to average plasma temperatures of 1.7×10^4 and 2.0×10^4 K for pressures of 2.4×10^2 and 0.4×10^2 atm. respectively.

At shot-out, the railgun current was 34 kA and hence the plasma resistance was 4.4 mΩ. The microdensitometer reading close to shot-out showed no density or temperature variation and the plasma length was found to be

32 mm for the same light-intensity level as in the previous paragraph. Thus a value of 9.5×10^3 S/m is obtained for the electrical conductivity, which corresponds to average plasma temperatures of 1.3×10^4 and 1.4×10^4 K for pressures of 0.4×10^2 and 2.4×10^2 atm. respectively.

The temperature estimates reported here are all higher than the estimates obtained in Reference [23]. This is attributed to the fact that in Reference [23], the authors were studying a free-flowing plasma, i.e. a plasma without a projectile impeding its motion. In this situation, the plasma is longer and hence less dense than a typical plasma armature, which may account for the lower temperatures.

It should be noted that the estimates for the average internal temperature of the plasma armature have been determined by assuming that boundary effects between the rails and the plasma armature are negligible. When applying their one-dimensional arc dynamics code to the Rashleigh-Marshall experiment [31], Batteh and Powell found that the potential difference across the plasma was 47 V [17,18]. This value did not compare favourably with 160 V measured by Rashleigh and Marshall across the muzzle. They therefore concluded that boundary effects were important in explaining the muzzle voltage difference. In addition, Batteh and Powell found that the average plasma temperature was 5.6×10^4 K. They concluded that to obtain lower plasma temperatures, it was necessary to consider a two-dimensional model of the plasma armature in a railgun. However, their two-dimensional code [19,20] predicted plasma temperatures above 3.0×10^4 K. Although the railgun current given in Reference [31] was significantly higher than the current in the RPIP series, which would imply higher plasma temperatures, it is most likely Powell and Batteh's assumption that the plasma was nearly completely double-ionised was responsible for their very high temperature estimate.

Figure 26 shows the concentrations of copper, Cu^+ and Cu^{2+} predicted by Kovitya's code for the two pressures of 2.4×10^2 and 0.4×10^2 atm. between temperatures of 0.8×10^3 and 2.6×10^3 K. The graphs show that the concentration of neutral copper atoms decreases more rapidly for lower pressures as the temperature increases. In addition, the concentration of Cu^+ increases more rapidly for lower pressures until about 2.0×10^4 K. For temperatures above 2.0×10^4 K, the concentration of Cu^+ begins to decrease for the pressure of 0.4×10^2 atm. corresponding to an increase in the concentration of Cu^{2+}, whereas the concentration of Cu^+ at a pressure of 2.4×10^2 atm. is still increasing.

These results indicate that the concentration of neutral copper atoms can be significant for temperatures and pressures above 1.8×10^4 K and 240 atm. respectively. Furthermore, the concentration of Cu^+ may be significant at very high pressures for temperatures where the concentration of Cu^{2+} is significant at a pressure of 40 atm.

In the Rashleigh-Marshall experiment (hereafter referred to as the RM-experiment), the railgun current, the bore cross-section and L' were 300 kA, 1.6×10^{-4} m^2 and 0.42 μH respectively. Substituting these values into Equation (41) yields a pressure of 1.2×10^8 Pa or 1.2×10^3 atm, which is considerably higher than the pressures in the RPIP series. In view of the

results of the previous paragraphs, the concentrations of Cu and Cu^+ can be significant for temperatures above 2.0×10^4 K at a pressure of 1.2×10^3 atm. Using their two-dimensional model, Powell and Batteh [19,20] obtained an average plasma temperature of 3.7×10^4 K for the RM-experiment. Even at this temperature, it is most likely that the concentration of Cu^+ could be significant, thereby implying that the plasma is not completely double-ionised.

Powell and Batteh calculated a value of 50 V for the potential difference across the plasma, which was far below the 160 V measured across the muzzle in the RM-experiment. Using Equation (37) with l_a equal to 9.8 cm as given in Reference [21] yields a value of 4.8×10^{-5} Ωm for the plasma resistivity in the RM-experiment. The electrical conductivity is therefore 2.1×10^4 S/m, which corresponds to a temperature of 2.0×10^4 K for a pressure of 2.4×10^2 atm. according to Figure 24. The temperature is likely to be less than 2.0×10^4 K because using Equation (41) yields a pressure of 1.9×10^8 Pa or 1.9×10^3 atm for the RM-experiment. This implies that the plasma in the RM-experiment had significant contributions of Cu and Cu^+ and a negligible concentration of Cu^{2+}, which contradicts Powell and Batteh's assumption of the plasma being nearly completely double-ionised. It is also interesting to note that the temperature is not a strong function of the railgun current since the plasma temperature estimate for the RM-experiment did not increase by the same factor as the railgun current did, when compared with RPIP06.

5.9 Rail Damage

The damage to the inner surfaces of the rails caused by the plasma armature and runaway arcs was so severe that both rails had to be replaced after each firing. In this section a short summary on rail damage is presented. For a more complete description of damage in a RAPID railgun, especially from a metallurgical point of view, the reader is referred to References [9] and [32]. In more recent work, Sadedin and Stainsby [33] have investigated rail damage in a three-stage railgun incorporating puff-switching.

Two different forms of surface degradation were observed on the inner surfaces of the rails. The first of these was melting, which resulted in the ablation of material due to ordinary heat conduction occurring in the rails close to the inner surfaces. The second was related to arc damage which is discussed later. Melting is the more severe form of rail damage but is reduced when the projectile is injected into a railgun at high velocities [34].

The mechanism of heat-flow from the plasma armature to the rails is still not understood although Powell [35] has recently proposed a model for thermal energy-transfer in which it is assumed that the dominant heat-flow mechanism is radiation from the plasma armature impinging on the inner rail surfaces. Thus the heat-flux incident on the inner rail surfaces in this model is given by Equation (34).

When the plasma armature becomes relatively fast-moving, which occurs for displacements greater than 350 mm or for velocities greater than 700 m/s in a 6 kV firing using a RAPID railgun, there is not a sufficiently long exposure-time for melting to occur on the inner rail surfaces. Then the second form of surface degradation begins to appear.

The second form of surface degradation is known as 'arc damage'. The appearance of arc streaks or tracks on the inner surfaces of the rails, as described in Reference [9], is representative of this form of damage. Arc damage probably occurs throughout an entire firing and is most likely caused by the railgun current passing from the inner rail surface to the plasma armature on one side and then by the current passing from the plasma armature to the other inner rail surface. Since arc damage is not as severe as melting, it is likely that less material is ablated from the rail surfaces into the plasma armature for displacements greater than 350 mm. This implies that less rail material enters the plasma armature later in a firing.

It was observed that the arc track patterns on the two rails were different. This suggests that the current passing from one inner rail surface to the plasma armature does not behave in fine detail in the same way as the current passing from the plasma to the other inner rail surface. Thus the boundary conditions for the solution of the current diffusion equation, which will determine the current distribution in the rails, may be different for the respective rails. Hence it is probable that the resulting current distributions in both rails are different, thereby implying asymmetry. In previous calculations of the rail inductance [10,36], it has been assumed that the current distributions in both rails were the same.

6. EVALUATION OF RAILGUN PARAMETERS

6.1 Railgun Efficiencies

In this section an expression, which is not explicity dependent on barrel length, is derived for an upper bound to the efficiency of a railgun. The resulting expression is then compared with the exit-velocity measurements presented earlier. When the length of the gun barrel is explicity taken into account, the upper bound is reduced.

The single-shot efficiency of a railgun is usually defined as the ratio of the exit kinetic energy of the projectile to the initial input energy stored by the capacitor bank. Therefore the upper bound for the efficiency is found by determining the maximum possible exit-velocity. To calculate the maximum possible exit-velocity, Equation (31) is used with the retarding force term f set equal to zero. Thus in the capacitively-driven stage Equation (31) becomes:

$$(m_a + m_p)\frac{dv}{dt} = \frac{1}{2} L_p' I_m^2 e^{-R_{tot}t/L_o} \sin^2((1/L_oC - R_{tot}^2/4L_o^2)^{1/2}t) \qquad (42)$$

where use has been made of Equation (6). Integrating Equation (42) with respect to time yields:

$$(m_a + m_p)v = \frac{1}{2} L_p' I_m^2 \left(\frac{(1 - e^{-Rt/L_o})}{2R/L_o} + \frac{L_o C\, e^{-Rt/L_o}}{4} \left(\frac{R}{2L_o} \cos\left(2\left(\frac{1}{L_o C} - \frac{R^2}{4L_o^2}\right)^{1/2} t\right)\right.\right.$$

$$\left.\left. - \left(\frac{1}{L_o C} - \frac{R^2}{4L_o^2}\right)^{1/2} \sin\left(2\left(\frac{1}{L_o C} - \frac{R^2}{4L_o^2}\right)^{1/2} t\right) - \frac{RC}{8}\right) \right. \quad (43)$$

where the subscript 'tot' has been dropped for convenience. Equation (43) provides a value for the maximum projectile velocity at time t, when the railgun is being capacitively-driven provided the value used for L_p' is a maximum. To obtain the corresponding displacement at time t, Equation (43) must be integrated with respect to time. This yields:

$$(m_a + m_p)(x - x_o) = \frac{1}{2} L_p' I_m^2 \left[\frac{L_o t}{2R} - \frac{L_o^2(1 - e^{-Rt/L_o})}{2R^2} - \frac{RCt}{8}\right.$$

$$+ \frac{L_o^2 C^2}{16} \left(\frac{R}{2L_o} e^{-Rt/L_o} \left(-\frac{R}{L_o} \cos\left(2\left(\frac{1}{L_o C} + \frac{R^2}{4L_o^2}\right)^{1/2} t\right) + \right.\right.$$

$$\left.\left. 2\left(\frac{1}{L_o C} - \frac{R^2}{4L_o^2}\right)^{1/2} \sin\left(2\left(\frac{1}{L_o C} - \frac{R^2}{4L_o^2}\right)^{1/2} t\right)\right) + \frac{3R^2}{4L_o^2} - \frac{1}{L_o C}\right.$$

$$\left. - \left(\frac{1}{L_o C} - \frac{R^2}{4L_o^2}\right)^{1/2} e^{-Rt/L_o} \left(-\frac{R}{L_o} \sin\left(2\left(\frac{1}{L_o C} - \frac{R^2}{4L_o^2}\right)^{1/2} t\right) - \right.\right.$$

$$\left.\left. \left(\frac{1}{L_o C} - \frac{R^2}{4L_o^2}\right)^{1/2} \cos\left(2\left(\frac{1}{L_o C} - \frac{R^2}{4L_o^2}\right)^{1/2} t\right)\right)\right] \quad (44)$$

where x_o is the initial position.

In the early part of the inductively-driven stage it was found that the current in the RAPID railgun could be described by Equation (19).

term f set again equal to zero and then integrating with respect to time gives the following equation for the velocity of the plasma-projectile system:

$$(m_a + m_p)\,(v - v(t_c)) = \frac{L_o L_p' I_o^2}{4R_1}\,(1 - e^{-2R_1(t-t_c)/L_o}) \qquad (45)$$

where R_1 equals $R + R_{S_2}$ and $v(t_c)$ is the velocity at the instant the capacitor bank is crowbarred.

In the late part of the inductively-driven stage, typically for $t > 550$ μs from shot-start, it was found that the current in the railgun circuit was no longer described by Equation (20) because the total circuit resistance began to increase. For times greater than 550 μs, Equation (24) is more appropriate than Equation (20). However, since the current is exponentially-damped more in the late part of the inductively-driven stage than in the early part, Equation (45) is also applicable to this part of the inductively-driven stage.

The projectile displacement is obtained by integrating Equation (45) with respect to time and is given by:

$$(m_a + m_p)\,(x - x(t_c) - v(t_c)(t-t_c)) = \tfrac{1}{2} L_p' \left[\frac{L_o I_o^2 (t-t_c)}{2R_1} + \left(\frac{L_o I_o}{2R_1}\right)^2 (e^{-2R_1(t-t_c)/L_o} - 1)\right] \qquad (46)$$

where $x(t_c)$ is the projectile displacement at $t=t_c$ and is found by using Equation (44). Equation (46) has also been obtained independently by Batten [37] in a slightly different form.

An expression for an upper bound to the efficiency can now be derived from Equations (43) and (45). Firstly, a limiting velocity is obtained by considering the large-time limit, i.e. $t \to \infty$, in Equation (45). Thus the upper bound to the velocity attained by a projectile in a railgun is:

$$v_{max} = v(t_c) + \frac{L_p' L_o I_o^2}{4R_1 (m_a + m_p)} \qquad (47)$$

where the velocity $v(t_c)$ is found from Equation (43) and is given by:

$$v(t_c) = \frac{1}{2}\frac{L_p' I_m^2}{(m_a + m_p)}\left(\frac{1 - e^{-Rt_c/L_o}}{2R/L_o} + \frac{L_o C\, e^{-Rt_c/L_o}}{4}\left(-\left(\frac{1}{L_o C} - \frac{R^2}{4L_o^2}\right)^{1/2} \times \right.\right.$$

$$\left.\left.\sin\left(2\left(\frac{1}{L_o C} - \frac{R^2}{4L_o^2}\right)^{1/2} t_c\right) + \frac{R}{2L_o}\cos\left(2\left(\frac{1}{L_o C} - \frac{R^2}{4L_o^2}\right)^{1/2} t_c\right)\right) - \frac{RC}{8}\right) \qquad (48)$$

The upper bound velocity given by Equation (47) is not explicity dependent on the length of the gun-body but is dependent on the conditions in the railgun circuit at the instant when the capacitor bank is crowbarred. Equation (47) also requires that the combined mass of the plasma-projectile system be known. However, if the projectile exit time t_e is known, then the upper bound velocity is reduced to:

$$v_{max}(t_e) = v(t_c) + \frac{L' L_o I_o^2}{4R_1(m_a + m_p)}\left(1 - e^{-2R_1(t_e - t_c)/L_o}\right) \qquad (49)$$

which follows directly from Equation (45). The exit time is dependent on the length of the gun barrel amongst other parameters. From Equation (49), it can be seen that the longer it takes the projectile to reach its exit the higher the upper bound velocity becomes. Thus the upper bound velocity would be higher for the firings of longer duration in the RPIP series even though the measured exit velocities in these firings were considerably lower than the exit velocities measured in the experiments of shorter duration. Hence, it is more convenient to consider Equation (47) rather than Equation (49) because of its independence of the length of the gun barrel and the exit time t_e.

In order to determine the upper bound velocity given by Equation (47) for a RAPID railgun of arbitrary length, the value of L_p' is set equal to 0.53 μH/m. The value of 0.53 μH/m corresponds to an L'- value for a railgun with a rail height/bore width ratio of about 3/2. This value has been obtained by assuming that the current is distributed in thin sheets along the inner surfaces of the rails [10]. Since diffusion of current into the rails has not been allowed for, the value chosen for L_p' is considered to be a maximum, thereby ensuring that Equation (47) is truly an upper bound.

Before the upper bound velocity in Equation (47) can be obtained, the velocity $v(t_c)$ must be found. In the RPIP series the time at which the capacitor bank was crowbarred was about 190 μs after shot-start. The value of I_m is found by using Equation (15) with I_p equal to 81 ± 8 kA. Using the RPIP02 values for τ and ω in Table 3 yields a value of 89 ± 9 kA for I_m. Putting $(m_a + m_p)$ equal to 0.39 g in Equation (48) yields a value of (5.0 ± 1.1) x 10^2 m/s for $v(t_c)$.

At $t = t_c$, the experimental value for railgun current I_o was 77 ± 8 kA. When this value is introduced into Equation (47) along with the value of (t_c), a value of (2.1 ± 0.5) x 10^3 m/s is obtained for v_{max}. Since the exit

time for the RPIP series was less than 1 ms, $v_{max}(t_e)$ found from Equation (47) is $(1.9 \pm 0.4) \times 10^3$ m/s for t_e equal to 1.0 ms. As expected, both velocities v_{max} and $v_{max}(t_e)$ are much greater than the exit velocities appearing in Table 2, which do not even reach 1 km/s except for some dubious results. A comparison of the maximum exit velocity $v_{max}(t_e)$ with the exit velocity recorded for RPIP02 (923 m/s) gives an indication of the substantial effect on railgun performance caused by retardational effects and/or by the diffusion of current in the rails, which can lower the value of L' substantially [10].

The efficiency of a railgun is defined as the ratio of the kinetic energy of the projectile on exit to the total energy initially stored by the capacitor bank. Therefore, using Equation (47), the upper bound to the efficiency, denoted by ϵ_{max}, is:

$$\epsilon_{max} = \frac{m_p L'^2}{4C(m_a + m_p)^2 v_o^2} \left(I_m^2 \gamma + I_o^2 L_o/2R_1\right)^2 \tag{50}$$

where the parameter γ is given by:

$$\gamma = 2 (m_a + m_p) v(t_c)/L' I_m^2 \tag{51}$$

The energy stored by the capacitor bank can be related to the energy stored by the inductor at peak current by the following equation:

$$CV_o^2 = \beta L_o I_p^2 \tag{52}$$

where β is greater than or equal to unity. When β equals unity, all the energy in the capacitor bank is transferred to the storage inductor at peak current, i.e. the railgun behaves as an LC-oscillator. As discussed in Subsection 5.2, β is greater than unity for a RAPID railgun and is approximately equal to 1.4 assuming the calibration factor for the current-time records is 92 kA/V.

If Equations (15) and (52) are introduced into Equation (50), then an alternative form for the upper bound to the efficiency is:

$$\epsilon_{max} = \frac{m_p L'^2}{4\beta L_o (m_a + m_p)^2} \left(\gamma I_p \exp(R\pi/2\omega L_o) + L_o I_o^2 /2R_1 I_p\right)^2 \tag{53}$$

If the dependence on the time taken for the projectile to exit (t_e) is included, as in Equation (49), then Equation (53) becomes:

$$\eta_{max} = \frac{m_p L'^2}{4\beta L_o (m_a + m_p)^2} \left(\gamma I_p e^{R\tau/2\alpha L_o} + \frac{L_o I_o^2}{2 I_p R_1} \left(1 - e^{-2R_1(t_e - t_c)/L_o}\right)\right)^2 \qquad (54)$$

It should be noted that Equations (50) and (53) are not valid for small values of R_1, i.e. when

$$R_1 \leq \frac{L_o I_o^2}{2 I_p} \left(\frac{2(m_a + m_p)}{L'} \left(\frac{\beta L_o}{m_p}\right)^{1/2} - \gamma I_p \exp\left(\frac{R\tau}{2\alpha L_o}\right)\right)^{-1} \qquad (55)$$

Substituting the values found earlier for RPIP02 and a value of 0.53 μH/m for L' into the inequality indicates that Equations (50) and (53) are not valid for a RAPID railgun when the circuit resistance in the inductively-driven stage is less than 1.1 mΩ . This did not occur in the RPIP series (see Table 3). According to Figure 8, a value of 1.1 mΩ is a factor of 2 to 5 less than the resistance of the plasma armature. Thus for the unlikely situation where the inequality is valid, the duration of the railgun firing should be considered when evaluating the upper bound to the efficiency. Hence Equations (51) and (54) should be used instead.

The equations for the upper bound in the efficiency, i.e. Equations (50), (53) and (54), indicate that the efficiency depends on the square of the rail inductance per unit length and on the square of the peak current. In addition, the second term on the right hand side of Equation (53) for a RAPID railgun dominates the first term, which is valid for all inductively-driven guns. It is interesting to note that an increase in L' is just as effective as increasing the peak current in order to improve the efficiency of a railgun. An increase in L' implies altering the geometry of the railgun to increase the total magnetic flux between the rails. This can be done by increasing the rail separation and/or by decreasing the height of the rails. An increase in the peak current, however, is limited by the maximum amount of energy capable of being stored by the capacitor bank.

For a RAPID railgun and using the circuit values for RPIP02, the upper bound to the efficiency given by Equation (50) yields a value of 0.030 ± 0.016 whereas the value for the efficiency given by Equation (54) is found to be 0.025 ± 0.011. As expected, these values are much higher than the experimental value of 0.007 for the efficiency given in Subsection 5.1.

It has already been shown that an increase in the efficiency of an electromagnetic launcher is achieved when the rail inductance per unit length and the peak current are increased. An increase in efficiency will also occur when the mass of the plasma-projectile system and total circuit resistance are as low as possible. In addition, an increase in efficiency will result if β can be made to approach unity.

The equations presented in this section highlight the importance of the time constant τ. As can be seen from the experimental results, it is the inductively-driven stage which is responsible for the dominant contribution to the exit velocity of the projectile. Thus the larger the time constant, the

more efficient the firing. Hence it is necessary to keep the circuit resistance as low as possible. If possible, techniques aimed at stopping the resistance from increasing during firings as observed in Subsection 5.2 should be sought.

Since RPIP02 was amongst the most efficient of the firings in the series, those firings in Table 3 with significantly larger time constants than RPIP02 must be considered dubious unless crowbarring of the capacitor bank occurred at a lower value of I_o, i.e. later, or arcing occurred ahead of the projectile in those firings.

6.2 Lower Bound for the Effective Inductance Per Unit Length

In the previous subsection expressions for an upper bound to the velocity of a railgun projectile at any time t were obtained. These expressions, given by Equation (43) for $t < t_c$ and by Equation (45) for $t > t_c$, can be used to determine a lower bound to the effective inductance per unit length for each firing.

The effective inductance per unit length L'_{eff} is a quantity used to replace the right hand side of Equation (31) to the more convenient form of:

$$(m_a + m_p)\frac{dv}{dt} = \frac{1}{2} L'_{eff} I^2 \qquad (56)$$

where $L'_{eff} = L' - 2f/I^2$. If L'_{eff} is assumed to be constant in a railgun firing, a lower bound to it is found by replacing L'_p in Equations (43) and (45) by L'_{eff} and then equating the right hand side of Equation (45) with t replaced by t_e to the experimentally-determined momentum of the plasma-projectile system on exit. Thus the lower bound to the effective inductance per unit length for a RAPID railgun firing is:

$$(L'_{eff})_{min} = \frac{4(m_a + m_p)\, v_e}{\tau I_o^2 (1 - e^{-2(t_e - t_c)/\tau}) + 4(m_a + m_p) v(t_c)/L'_p} \qquad (57)$$

where v_e is the measured exit velocity and $v(t_c)$ is given by Equation (43). In Equation (57), the time constant τ equals L_o/R_1. For RPIP02, $(m_a + m_p)$ was equal to 0.392 g, τ was equal to 8.3×10^{-4} s and I_o was equal to (77 ± 8) kA. In addition, $v(t_c)/L'_p$ was equal to $(9.4 \pm 2.1) \times 10^8$ m^2/Hs and t_e was approximately equal to 770 ± 20 μs. Substituting these values and a value of 923 m/s for v_e into Equation (57) yields a lower bound for L'_{eff} of (0.28 ± 0.07) μH/m. Because of the large uncertainty in the lower bound for L'_{eff}, it is not possible to compare lower bound L'_{eff} values from different firings.

The lower bound to L'_{eff} is not expected to be much less than L'_{eff} because Equation (47) with L'_p replaced by L'_{eff} is valid for most of a RAPID

firing. Furthermore, if it is assumed that frictional effects in a railgun are negligible, then the propelling inductance per unit length is close to the lower bound for the effective inductance per unit length, i.e. the value for L'_p is about (0.28 ± 0.07) μH/m. Since the propelling inductance per unit length is close to the rail inductance per unit length L', a value of (0.28 ± 0.07) μH/m for L' indicates that significant diffusion of the current into the rails has occurred and/or that retarding effects on the plasma-projectile system are significant. However, it is not expected that significant diffusion of the current into the rails will occur in a RAPID firing [10], thereby implying that retarding effects such as atmospheric drag and friction due to the rails and RAPID gun-body are mainly responsible for the low values of the effective inductance per unit length.

6.3 Discussion Concerning Retardational Effects and the Parameter $L'_{eff}/(m_a+m_p)$

A basic factor appearing in railgun performance calculations is the ratio of the effective inductance per unit length L'_{eff} to the combined mass of the plasma-projectile system, $m_a + m_p$. The question of the constancy of the parameter $L'_{eff}/(m_a + m_p)$ is discussed in this subsection. It should be noted that if the parameter $L'_{eff}/(m_a + m_p)$ is constant, then Equations (42) to (48) with L'_p replaced by L'_{eff} become the equations describing railgun performance in the capacitively-driven stage and the early part of the inductively-driven stage.

Both the quadratic and cubic curve fits presented in Subsection 5.5 are better fits to the displacement-time results for RPIP02 than the analysis presented by Bedford [38], who has argued that a value of 6.8×10^{-4} H/kg for L'_{eff} adequately describes the displacement-time curve for RPIP02. In Subsection 5.5, it was also stated that the experimental data for the RPIP series were not sufficiently accurate to differentiate between a quadratic and a cubic displacement-time curve or even a higher order curve. A physical argument was presented to show that the acceleration predicted by the cubic curve would be more consistent with the expected acceleration for $t > 160$ μs than the acceleration predicted by the quadratic curve. However, the argument did not rule out the possibility that higher order polynomials, one applying to the capacitively-driven stage and another to the inductively-driven stage might be more appropriate.

If Equation (30) is sufficiently accurate to describe the displacement-time results of a railgun firing for $t > 160$ μs, then the following result is obtained from Equation (56):

$$\frac{L'_{eff}}{(m_a + m_p)} = \frac{2(6a_1 t + 2b_1)}{I(t)^2} \qquad (58)$$

The current I(t) behaves as a damped sinusoid in the capacitively-driven stage and an exponentially-decaying function in the inductively-driven stage. Thus Equation (58) demonstrates that the parameter $L'_{eff}/(m_a + m_p)$ is a time-varying function with values ranging from 2.0×10^{-4} to 7.3×10^{-4} H/kg for RPIP02.

Furthermore, since the mass of the projectile was considerably larger than the mass of the foil for most of the RPIP firings, much of the time variation in $L'_{eff}/(m_a + m_p)$ should be due to L'_{eff}. A time-varying effective inductance per unit length means that the propelling inductance per unit length L'_p is time-varying and/or that retardational effects are not proportional to $I(t)^2$ alone.

An estimate for the retardational force f acting against the plasma-projectile system can be obtained by differentiating Equation (30) twice with respect to time and then substituting the resulting expression for the acceleration into Equation (31). This yields:

$$f \sim \frac{1}{2} L'_p I^2 - 2(m_a + m_p)(3a_1 t + b_1) \qquad (59)$$

The cubic displacement-time curve has been chosen because the acceleration obtained from this curve decreases for t > 160 μs from shot-start which is expected because the railgun current decreases to less than half its maximum value over the duration of a RAPID firing.

For RPIP02, the coefficients a_1 and b_1 are given in Table 4 as $(-1.5 \pm 0.5) \times 10^8$ m/s^3 and $(7.4 \pm 0.6) \times 10^5$ m/s^2 respectively. Putting L'_p, $(m_a + m_p)$ and I equal to 0.40 μH/m [36], 0.39×10^{-3} kg and 81 kA yields a value of $(7.9 \pm 0.7) \times 10^2$ N for f. Putting I equal to 60 kA and t equal to 3.3×10^2 μs (see Figure 4) yields a value of $(2.6 \pm 0.9) \times 10^2$ N for f. These results indicate that retardational effects are not only significant but that they also decrease over the duration of a firing.

To confirm the behaviour observed in the previous paragraph, the same analysis is applied to another successful firing RPIP06. The coefficients a_1 and b_1 are given in Table 4 as $(-2.0 \pm 0.5) \times 10^8$ m/s^3 and $(8.1 \pm 0.5) \times 10^5$ m/s^2 respectively. Using the same values for L'_p and $(m_p + m_a)$ and putting I equal to its maximum value of 81 kA yields a value of $(7.6 \pm 0.6) \times 10^2$ N for f. Putting I equal to 60 kA and t equal to 3.3×10^2 μs yields a value of $(2.4 \pm 0.8) \times 10^2$ N for f, thereby confirming the behaviour found in RPIP02.

Since the retardational force f in Equation (59) is expected to be greater than zero, it follows that

$$I > \left(\frac{4(m_a + m_p)(3a_1 t + b_1)}{L'_p} \right)^{1/2} \qquad (60)$$

Thus to fit a cubic displacement-time curve to experimental data, the recorded current I must be greater than the minimum value obtained from the right hand side of the above inequality. This minimum value occurs when t is equal to t_e since a_1 and b_1 were respectively negative and positive for the RPIP series.

For RPIP02, t_e was found to be 770 ± 20 μs. Putting t, a_1 and b_1 equal to 790 μs, -1.5×10^8 m/s^3 and 7.4×10^5 m/s^2 respectively and using the same values for L'_p and $(m_a + m_p)$ as before yields a minimum value of 39 kA for the right hand side of the inequality. However, at exit the recorded

current I was found to be 34 kA (Figure 4). (This suggests from Equation (59) that f is negative.)

It could perhaps be argued that a different cubic displacement-time curve involving the minimum values for a_1 and b_1 in Table 4 should be used in order to obtain lower values for the right hand side of the inequality at $t=t_e$. That is, a_1 and b_1 should equal -2.0×10^8 m/s^3 and 6.8×10^5 m/s^2 with c_1 and d_1 equal to their largest possible values of 10.7×10^1 m/s and -1.9×10^{-3} mm respectively. Although these values yield a minimum value of 29 kA for $t = 790$ μs, the displacement using this curve is found to be 4.1×10^2 mm, which is about 40 mm below the actual displacement at shot-out. Hence the cubic displacement-time curve given by the alternative values for a_1, b_1, c_1 and d_1 does not fit the experimental displacement-time data accurately and therefore cannot be used to describe railgun performance for RPIP02. Thus it is most likely that the minimum value of 39 kA obtained for the right hand side of the inequality is correct. It should be noted that using the quadratic displacement-time curve for RPIP02 yields a higher minimum value for the right hand side of the inequality (~47 kA).

Three explanations can be given for the recorded current falling below the minimum value obtained for the right hand side of the inequality. The first, which may only be a partial explanation, is that the current-time records were not calibrated correctly. A second explanation is that the L_p'-values considered in this subsection were not high enough. It has been assumed here that L_p' is closely equal to L', which is believed to be about 0.40 μH/m for a RAPID railgun according to Reference [36]. Higher values for L_p' would imply that the estimates for the retardational force f were greater than the estimates obtained earlier. The third explanation is that there may be an additional term propelling the plasma-projectile system, which might be due to the explosion of the metallic foil.

7. ARCING AHEAD OF THE PROJECTILE

In this section the phenomenon of arcing ahead of the projectile is studied to understand its effect on railgun performance. An example of a runaway arc is shown in Figure 13. In this figure it can be seen that the runaway arc increases its length during acceleration whereas the length of the plasma armature immediately behind the projectile decreases. Once the runaway has made its exit, which occurs in this example about 0.3 ms after shot-start, the length of the plasma armature increases suddenly. In addition, it should be noted that arcing ahead of the projectile was more likely to occur when the lighter pieces of foil were used to generate the plasma armature.

An explanation for the behaviour described in the previous paragraph is as follows. If the current in, and resistance of, the plasma armature are given by I_1 and R_a respectively, then the potential difference across the plasma is R_aI_1. If the current passing through the runaway arc is given by I_2, then the potential difference across it will be R_rI_2 where R_r is the resistance of the runaway arc. By applying Kirchhoff's law, the following equation is obtained:

$$R_a I_1 \sim R_r I_2 + R'(x_2 - x_1)I_2 + \frac{d}{dt}(L'(x_2 - x_1)I_2) \qquad (61)$$

where x_2 and x_1 are the displacements of the runaway arc and plasma-projectile system respectively. In obtaining Equation (61) it has been assumed that the total electrode potential difference of the plasma armature is approximately equal to the total electrode potential difference of the runaway arc. The various terms in Equation (61) are now examined to see if a simpler form is permissible.

To show that the inductive term in Equation (61) does not dominate, this term is evaluated when it is expected to be greatest, i.e. when the runaway arc has reached the muzzle. In many of the RPIP firings with arcing ahead of the projectile, the runaway arc had reached the muzzle during the early part of the inductively-driven stage. Assuming that the runaway arc was created soon after shot-start, an estimate for the maximum average rate of change of I_2 can be obtained by dividing the total railgun current at exit of the runaway arc by the life-time of the runaway arc Δt. For $\Delta t < t_c$, dI_2/dt can be approximated by $I_m \exp(-R_{tot} t/2L_o) \sin((L_o C)^{-1/2} t)/\Delta t$ and for $\Delta t > t_c$ which applies to RPIP19, dI_2/dt can be approximated by $I_o \exp(t_c - \Delta t)/\Delta t$. Thus for $\Delta t > t_c$, the induced emf e given by the inductive term in Equation (61) can be written as:

$$e \sim L' ((v_2 - v_1) I_2 + (x_2 - x_1) I_o \exp (t_c - \Delta t)/\Delta t) \qquad (62)$$

where v_2 and v_1 are respectively the velocities of the runaway arc and plasma armature. Thus to show that the right hand side of Equation (62) is not significant, estimates for the exit velocity of the runaway arc and for the displacement and velocity of the plasma projectile system are required.

Using the streak photograph for RPIP19, the values of v_2, v_1, Δt and x_1 were found to be about 2.8 km/s, 4.7×10^2 m/s, 0.30 ms and 90 mm respectively. Therefore using values of 7.9×10^{-4} s and 0.40 μH/m for t_c and L', the induced emf e is approximately equal to $9.2 \times 10^{-4} I_2 + 9.6 \times 10^{-3}$. The value of 9.6×10^{-3} can be neglected since values of I_2 are expected to exceed 10^2 A. The value of 9.2×10^{-4} is an equivalent resistance arising from the inductive term in Equation (61) and is almost an order of magnitude lower than the cicuit resistance given in Table 3 for RPIP19.

To show that resistive effects due to the rails are not significant in Equation (61), the resistance $R'(x_2 - x_1)$ must be evaluated. The resistance per unit length of a pair of rails is given by:

$$R' = 2 \rho_{rail}/A \qquad (63)$$

where ρ_{rail} is the average resistivity of the rail material and A is the cross-sectional area of the rails. In Equation (63) it has been assumed that the current has fully penetrated the rails, which may not be valid for a RAPID railgun [11]. The resistivity of the rail material used in the RPIP series

was approximately 2.5×10^{-8} Ωm while the cross-sectional area was about 1.6×10^{-4} m^2. Hence R' is about 3.1×10^{-4} Ωm^{-1}. Since the value for the displacement between the runaway arc on exit and the plasma-projectile system in Figure 13 is about 0.36 m, the estimated resistance due to the resistivity of the rails in Equation (61) is approximately 1.1×10^{-4} Ω, which is also an order of magnitude lower than the total resistance of the railgun circuit.

Using the values derived above, Equation (61) at the exit of the runaway arc becomes:

$$R_a I_1 \simeq R_r I_2 + 1.0 \times 10^{-3} I_2 \qquad (64)$$

In order to show that the second term on the right hand side of Equation (64) does not dominate the first term on that side, an estimate for the resistance of the runaway arc R_r is required.

The required estimate can be made by using the muzzle voltage record for RPIP19 shown in Figure 16. Here the voltage decreases only marginally throughout the firing except when the runaway arc leaves the railgun about 0.3 ms after shot-start. The exit of the runaway arc took about 0.15 ms. Prior to the exit of the runaway arc, the average muzzle voltage was about 170 V. According to Reference [12], the cathode electrode drop is about 7.5 V while that for the anode may range from 0 to 7 V. Therefore, allowing 15 V for the total electrode potential drop yields a value of about 155 V for the potential difference across the runaway arc. Since the maximum current in the RPIP series was 81 ± 8 kA, the minimum resistance across the runaway arc is found to be 1.9 ± 0.2 mΩ. Hence the second term on the right hand side of Equation (64) is a factor of almost 2 to 2.5 less than the first term. In Equation (61), if ε is equal to the ratio of the voltage due to the rails to the potential across the runaway arc, then Equation (64) becomes:

$$R_a I_1 \simeq (1 + \varepsilon) R_r I_2 \qquad (65)$$

where ε varies between 0 and 0.5 corresponding respectively to the creation and ejection of the runaway arc. Thus the contributions due to the rails in Equation (61) have only a marginal effect.

The resistances of the plasma armature and runaway arc are given by Equation (28). Using the appropriate forms of Equation (28) for R_a and R_r gives:

$$\frac{I_1}{l_a} \simeq (1+\varepsilon) \frac{\eta_r I_2}{\eta_a l_r} \qquad (66)$$

where η_a and l_a are the average resistivity and length of the plasma armature respectively. The subscript 'r' denotes the same physical quantities for the runaway arc.

Because the total railgun current is equal to $I_1 + I_2$ and does not vary significantly over the life-time of the runaway arc, a sudden decrease in I_1 means an increase in I_2. If the ratio of the two resistivities in

Equation (66) is assumed not to vary significantly, i.e. the density and temperature of both the runaway arc and plasma armature do not vary greatly over the life-time of the runaway arc, then it follows from Equation (66) that as I_1 decreases, and I_2 increases, the length of the plasma armature l_a decreases and the length of the runaway arc increases. This is the behaviour observed on the streak record for RPIP19 and confirms that the first term on the right hand side of Equation (61) dominates the second term. Thus the length of the runaway arc increases during acceleration because a greater amount of the total railgun current is being continually drawn away from the plasma armature by the runaway arc. Hence, the electrical conductivity of the runaway arc is higher than the electrical conductivity of the plasma armature, which occurs as a result of the runaway arc's lower density. The density of the plasma armature is greater than that of the runaway arc because the plasma armature is being impeded by the projectile. As I_1 decreases, the propelling force on the plasma-projectile system decreases and railgun performance is affected. The behaviour described in this paragraph means that when arcing occurs ahead of the projectile, it is not valid to assume that a constant fraction of the total current is drawn by the runaway arc as was done in the PARA code.

After the runaway arc has left the railgun, the current passing through the plasma armature increases suddenly. The muzzle voltage reverts to its previous value and hence the new ratio of the current passing through the plasma armature to the plasma length will equal approximately the value obtained from either side of Equation (66). Thus the sudden increase in current passing through the plasma armature causes a sudden increase in plasma length, which is shown in Figure 16.

A comparison of the projectile exit-velocities for RPIP02 and RPIP12 with that for RPIP19 can be made since the same gun-body and aluminium foil masses were used in all three firings. The comparison is particularly useful because it provides an indication of the effect that arcing ahead of the projectile has on railgun performance, bearing in mind that there was little leakage and no plasma disruption on the streak records for RPIP02 and RPIP12.

Since the exit velocity for RPIP02 was about the same as that for RPIP12 and was measured as 923 m/s, the kinetic energy of the projectile on exit was approximately 166 J. The kinetic energy of the projectile on exit for RPIP19 was about 98 J. Thus arcing ahead of the projectile has resulted in a 40% reduction in the projectile's kinetic energy.

The results presented in this section are now used to obtain an estimate of the runaway arc's mass and density on exit. If it is assumed that when arcing occurs ahead of the projectile, a negligible amount of energy is lost in the rails due to the current ahead of the projectile, then the difference in the kinetic energies between RPIP02 and RPIP19 can be used as a guide to the kinetic energy of the runaway arc. Although energy is lost due to ohmic heating in the rails, the estimate for the runaway arc's mass determined in this manner will be an upper bound. Since the velocity of the runaway arc was found to be 2.8 km/s on exit, the mass of the runaway arc will not be greater than 1.6×10^{-2} g, which is the same order of magnitude as the mass of the aluminium foil used in all three experiments ($\sim$ 0.012 g). The volume of the runaway arc on exit was approximately 5.6×10^{3} mm^3. Thus the density of the runaway arc is about 2.9 kg/m^3 for a mass of 1.6×10^{-2} g.

This indicates that the density of a runaway arc can be a factor of 2.5 less than the density of the plasma armature.

8. DISCUSSION OF RESULTS

In this section some of the aims of the RPIP series listed in Section 3 are discussed.

8.1 Performance Results

In the RPIP series, it was possible to photograph events during firings by using the transparent gun-body known as RAPID. Although two types of photograph were taken in the series, it was found that the streak photographs were more useful than the framing photographs because projectile displacements and plasma lengths could be obtained from the streak photographs. The only useful information obtained from the framing photographs was that plasma leakage occurred in every RPIP firing. Plasma leakage did not appear on all streak photographs because the neutral density filter on the streak camera accepted a narrower range of light than the filter on the framing camera.

The analysis presented in Subsection 5.5 indicates that either a quadratic or a cubic displacement-time curve can satisfactorily describe the displacement-time data within experimental error. The results in Table 4 show that the acceleration obtained from the quadratic displacement-time curve ranged from $(6.5 \pm 0.2) \times 10^5$ m/s^2 for RPIP10 to $(11.2 \pm 0.6) \times 10^5$ m/s^2 for RPIP02. Lower values for the acceleration were mainly due to arcing occurring ahead of the projectile.

Although the displacement-time data were more accurate and numerous than those previously obtained using position coils [6], it was not possible to distinguish whether the data followed a quadratic or a higher order displacement-time curve even allowing for the uncertainties in the coefficients. In order to find which curve-fits are appropriate for the capacitively-driven stage and for the inductively-driven stage, the displacement-time data must be more accurate than the data presented in this report. Only then will differentiation of the displacement-time curves or evaluation of central differences of the displacement-time data give sufficiently accurate information concerning the velocity-time profile of the plasma-projectile system in a railgun. The displacement data can be made more accurate by considering greater enlargements of the streak film and by placing position markers at various positions along the gun barrel. Errors or uncertainties in the time data could perhaps be reduced by having detectors such as breakwires placed close to the initial position of the projectile and at various positions along the gun-barrel.

8.2 Anomalous Effects

The three anomalous effects of plasma leakage, arcing ahead of the projectile and plasma disruption overshadowed any possible effects due to

particular types and masses of foil. The first two effects can have a substantial effect on railgun performance. For instance, the velocity between the lead-break and the breakscreen for RPIP01, which was a firing with much plasma leakage, was found to be 742 m/s. The corresponding velocity for RPIP02 (the most successful firing in the RPIP series) was found to be 860 m/s. Thus a 25 percent reduction in kinetic energy of the projectile can occur due to plasma leakage. In RPIP19, which had arcing ahead of the projectile, the flash-to-beam velocity was 731 m/s compared with 923 m/s for RPIP02. Thus a 40 percent reduction in the kinetic energy of the projectile can occur due to arcing ahead of the projectile. In RPIP15, which had one of the longest periods of plasma disruption lasting about 0.25 ms, the flash-to-beam velocity was found to be 880 m/s. This corresponded to a 10 percent reduction in the kinetic energy of the projectile compared with RPIP02, assuming that the mass and type of foil had a negligible effect on performance.

As mentioned earlier, the three anomalous effects could be detected on the muzzle and breech voltage records. Plasma disruption was characterized by sudden fluctuations appearing on the records whereas noisiness on the records corresponded to plasma leakage. A sharp peak appearing prematurely before shot-out on the voltage records meant that a runaway arc had been ejected from the railgun.

Plasma leakage and runaway arcs could also be detected on the time-of-arrival records and were responsible for many of the dubious flash-to-beam velocity results appearing in the second column of Table 2. Plasma leakage was responsible for producing high flash-to-beam velocities such as those for RPIP01 and RPIP13 and also for producing low velocities, e.g. RPIP11. In firings with much plasma leakage, it was difficult to decide when the projectile had left the railgun on the time-of-arrival records because the fibre-optic probe did not trigger properly. When a runaway arc is ejected, an early triggering of the fibre-optic probe occurs, thus leading to low flash-to-beam velocities being recorded for RPIP10, RPIP25 and RPIP26.

Although plasma leakage occurred in all of the RPIP firings, its effect on railgun performance was most noticeable in RPIP01 and RPIP26. Thus arcing ahead of the projectile, which occurred in 10 of the 26 firings, was the most serious of the three anomalous effects because of its frequency and greater effect on railgun performance.

Arcing probably occurs ahead of the projectile when a sufficient amount of plasma leaks past the projectile and enables current to be drawn away from the plasma armature. Because the RAPID gun-bodies of the RPIP series had been used extensively in previous firings, material ablated from the gun-bodies, particularly near the projectile's initial position, resulted in poor obturation. To stop the anomalous effects from occurring, railgun firings should be done with new gun-bodies.

8.3 Effect of Foil Mass and Type on Railgun Performance

As mentioned in Section 2, one of the predictions of the PARA code is that railgun performance is greatly affected by variations in the mass of the metallic foil used to generate the plasma armature. Although the foil

mass varied by a factor of 25 in the RPIP series, the projectile exit-velocities did not vary in the manner predicted by Richardson and Marshall [4]. Richardson and Marshall found that if the masses of the aluminium foil were 0.0104 and 0.036 g, then the projectile exit-velocities predicted by the PARA code were about 800 m/s and 1225 m/s respectively using similar electrical input energies to those used in the RPIP series. In the RPIP series the projectile exit-velocities for RPIP02 and RPIP12 were similar but the masses of the aluminium foil were 0.0117 and 0.0615 g respectively. The projectile exit velocities for RPIP04 and RPIP16 did not differ greatly (see Table 2), though the masses of zinc foil used in RPIP04 and RPIP16 were 0.0422 and 0.2006 g respectively. Similarly, the projectile exit velocities for RPIP06 and RPIP21 did not differ greatly, though the masses of copper foil were 0.0475 and 0.1972 g respectively. Therefore, the experimental results indicate that the foil mass does not affect railgun performance significantly for the range of masses considered in the RPIP series. The results also indicate that the foil type may have little effect on railgun performance although only three different types of metallic foil were used in the RPIP series.

Many of the breech and muzzle voltage records were different, particularly early in the firings. However, it was not possible to correlate foil mass or type with observed behaviour. In the analysis of the current-time records, different values for the time constant and resistance of the railgun circuit were found, but again these values could not be correlated with any specific foil mass or type.

9. CONCLUSION

In this report the experimental results of the RPIP series have been presented, analysed and shown to be consistent with much of the theoretical material presented in this report. In addition, comparisons with the theoretical predictions of the PARA code have indicated some of the weaknesses of the code. It has been shown that railgun performance and plasma length behaviour are not accurately predicted by the PARA code.

The analysis of the current-time records has shown that in the capacitively-driven stage the railgun current is described by an exponentially-damped sinusoid whereas in the inductively-driven stage the current decayed exponentially. It has also been found in the late part of the inductively-driven stage that the time constant of the railgun circuit did not remain constant. Much of this behaviour was attributed to the plasma resistance beginning to increase a few hundred microseconds after crowbarring of the capacitor bank. It has also been revealed that a 27% energy difference existed between the energy in the railgun at peak current and the initial input energy. Two possibilities are cited for the cause of this energy difference. The first is that the calibration factor used to determine values of the railgun current could have been erroneous and the second is that generating a plasma armature by exploding a metallic foil may require more energy than that estimated in Subsection 5.2.

Many more displacement-time data were obtained from the streak photographs than previously acquired by position coils. This enabled a curve-fitting analysis to be undertaken. Although accurate curve-fits were obtained, the displacement-time data were not sufficiently accurate to determine the order of the polynomial most appropriate for describing railgun performance. However, all the curves presented in Table 4 provided estimates for railgun performance. The uncertainties appearing in the coefficients of the curves mean that many similar curves are capable of fitting the displacement-time data.

Three anomalous effects, namely plasma leakage, arcing ahead of the projectile and plasma disruption, occurred frequently throughout the RPIP series. Each of these effects influenced railgun performance, the most serious being arcing ahead of the projectile. This effect was capable of reducing the projectile's kinetic energy on exit by an estimated 40 percent. The occurrence of each effect could also be detected on the breech and muzzle voltage records but not on the current-time records. Plasma leakage and arcing ahead of the projectile probably occurred because of the poor obturation of the RAPID gun-bodies.

Microdensitometer readings of the streak film yielded light intensity-profiles of the plasma armature. The intensity-profiles could not be calibrated to give plasma temperature estimates. However from these profiles, it was found that the plasma length was mostly between 25 and 45 mm, when the three effects described in the last paragraph were negligible.

Since the muzzle voltage was steady, or decreased marginally, in a firing with a well-behaved plasma armature, the average plasma temperature could be found by using the plasma length estimates and the Spitzer formula for the plasma resistivity. Assuming that the plasma armature was first-ionised, the average plasma temperature was estimated to be around 1.6×10^4 K reaching a maximum value around 2.6×10^4 K. It is unlikely that the plasma temperature reached 2.6×10^4 K because assuming the plasma behaved as a black-body only yielded a maximum temperature of $(2.1 \pm 0.1) \times 10^4$ K. These temperature estimates are considerably lower than the temperatures computed by Powell and Batteh [16-19]. A computer code developed by Kovitya [18,28] was also used to verify the low temperature estimates and yielded plasma temperatures of 1.7×10^4 and 2.0×10^4 K at pressures of 0.4×10^2 and 2.4×10^2 atm. respectively for a railgun current of 66 kA. For a railgun current of 34 kA, the plasma temperatures at pressures of 0.4×10^2 and 2.4×10^2 atm. were found to be 1.3×10^4 and 1.4×10^4 K respectively.

The analysis presented in this report has highlighted two major problem areas with regard to the viability of electromagnetic launchers. Firstly, even if retardational effects are neglected in a RAPID railgun, the upper bound for the exit velocity of the projectile is found to be 2.1 ± 0.5 km/s, which corresponds to an efficiency of 2-3 percent. When retardational effects are considered, the efficiency decreases significantly. The highest exit velocity measured in the RPIP series was just below 1.0×10^3 m/s. Thus retardational effects may be responsible for about a 70 percent reduction in the efficiency, assuming current diffusion into the rails is negligible.

Besides retardational effects, there are many other factors affecting railgun efficiency. An increase in efficiency is achieved by increasing the time constant τ of the railgun circuit. Thus a decrease in R_{tot} or an increase in L_o is desirable. Although low values ranging from 7 to 10 mΩ were obtained for the RAPID railgun resistance, these values were not low enough to produce large values for the time constant, which ranged from 7×10^{-4} to 9×10^{-4} s. In addition, the efficiency increases with the propelling inductance per unit length (L_p') and the peak current. Increasing the current density in the plasma armature will produce larger values for L_p' as well as increasing the magnetic field contribution due to the rails. The peak current can be increased by extending the capabilities of the power source. Finally, a more efficient transfer of the initial storage energy to the storage inductor results in increased railgun efficiency. All the factors mentioned in this paragraph affect the design of railguns.

The second problem area with regard to the viability of electromagnetic launchers is rail damage. In the RPIP series, the rail damage was so serious that the rails had to be replaced after each firing. The two different forms of surface degradation on the inner rail surface were melting of the rails, which occurred principally in the early stage of a firing and arc streaks, which appeared on the rails later in a firing. The more serious form of damage was melting and as a means of overcoming the severity of this problem it is suggested, based on Subsection 5.9, that a projectile moving with an initial velocity of at least 700 m/s should be injected into a RAPID railgun.

It was found that the mass and type of plasma-initiating foil did not have the significant effect on railgun performance predicted by the PARA code. Although diagnostic measurements were different from shot to shot, these differences could not be correlated with a specific mass or type of plasma-initiating foil.

10. ACKNOWLEDGEMENTS

The author wishes to thank Drs A.J. Bedford, R.A. Marshall, D.D. Richardson and D.R. Sadedin and Messrs G.A. Clark and D.F. Stainsby for several interesting and informative discussions. In addition, the assistance provided by Mr I. MacIntyre and the Explosives Instrumentation Group of MRL is gratefully acknowledged. The author wishes to thank Messrs W.A. Jenkins, B. Jones and M.E. Astill for providing the experimental details and results used in this report.

11. REFERENCES

1. Bedford, A.J., Clark, G.A. and Thio, Y.C. (1983). Experimental Electromagnetic Launchers at MRL. Report MRL-R-894. Materials Research Laboratories, Melbourne, Victoria, Australia.

2. Thio, Y.C. (1983). PARA: A Computer Simulation Code for Plasma Driven Electromagnetic Launchers. Report MRL-R-873, Materials Research Laboratories, Melbourne, Victoria, Australia.

3. Richardson, D.D. (1985). Spectroscopic Studies of a Railgun Muzzle Flash. Report MRL-R-952, Materials Research Laboratories, Melbourne, Victoria, Australia.

4. Richardson, D.D. and Marshall, R.A. (1983) Use of the Computer Program PARA 30 to Study Results from Firing the Railgun ERGS-1M. Report MRL-R-900, Materials Research Laboratories, Melbourne, Victoria, Australia.

5. Clark, G.A. and Bedford, A.J. (1984). Performance Results of a Small-Calibre Electromagnetic Launcher. IEEE Transactions on Magnetics Vol MAG-20, No. 2, 276.

6. Clark, G.A. and Bedford, A.J. (1984). Performance Results of a Small-Calibre Electromagnetic Launcher. Report MRL-R-917, Materials Research Laboratories, Melbourne, Victoria, Australia.

7. Kennett, S.R. (1984). The Interactive Plotting Program - GRAPH. Technical Note MRL-TN-485, Materials Research Laboratories, Melbourne, Victoria, Australia.

8. Stainsby, D.F. and Bedford, A.J. (1984). Some Diagnostic Interpretations from Railgun Plasma Profile Experiments. IEEE Transactions on Magnetics Vol MAG-20, No. 2, 332.

9. Bedford, A.J. (1984). Rail Damage in a Small Calibre Railgun. IEEE Transactions on Magnetics Vol MAG-20, No. 2, 348.

10. Kowalenko, V. (1986). Rail Inductance Calculations for Some Simple Current Distributions.Report MRL-R-976, Materials Research Laboratories, Melbourne, Victoria, Australia.

11. Kowalenko, V. (1986). The Magnetic Flux Contributed by the Plasma Armature in an Electromagnetic Launcher. Report MRL-R-1033, Materials Research Laboratories, Melbourne, Victoria, Australia.

12. Lafferty, J.M. (ed.) (1980). Vacuum Arcs, 1st Ed., (Wiley & Sons, NY,), p.14.

13. Kowalenko, V. (1986). Experimental Results from Railgun Firings Involving Magnetic Probes. Technical Note MRL-TN-509, Materials Research Laboratories, Melbourne, Victoria, Australia.

14. Spitzer, L. (1965). Physics of Fully Ionised Gases, (Interscience, New York), Chapter 5.

15. McCracken, D.D. and Dorn, W.S. (1964). Numerical Methods and Fortran Programming, 1st Ed., (Wiley & Sons, NY), p. 262.

16. Powell, J.D. and Batteh, J.H. (1983). Atmospheric Effects on Projectile Acceleration in the Rail Gun. J. Appl. Phys. 54, No. 12, 7195.

17. Batteh, J.H. and Powell, J.D. (1980). Plasma Dynamics of the Arc-Driven Rail Gun. Technical Report ARBRL-TR-02267, Ballistic Research Laboratory, Maryland, USA.

18. Powell, J.D. and Batteh, J.H. (1981). Plasma Dynamics of an Arc-Driven, Electromagnetic, Projectile Accelerator. J. Appl. Phys. 52, 2717.

19. Kovitya, P. (1985). Physical Properties of High-Pressure Plasmas of Hydrogen and Copper in the Temperature Range 5000 K to 30000 K. IEEE Transactions on Plasma Science PS-13, No. 6, 587.

20. Powell, J.D. (1982). Two-Dimensional Model for Arc Dynamics in the Rail Gun. Technical Report ARBRL-TR-02423, Ballistic Research Laboratory, Maryland, USA.

21. Powell, J.D. and Batteh, J.H. (1983). Two-Dimensional Plasma Model for the Arc-driven Rail Gun. J. Appl. Phys. 54, 2242.

22. Ichimaru, S. (1983). Basic Principles of Plasma Physics - A Statistical Approach, (W.A. Benjamin Inc., Reading, Massachusetts, USA), p.7.

23. Clark, G.A. and Kowalenko, V. Temperature Estimates for a Free Flowing Railgun Plasma. Report in preparation, Materials Research Laboratories, Melbourne, Victoria, Australia.

24. Spitzer, L. and Härm, (1953). Transport Phenomena in a Completely Ionized Gas. Phys. Rev. 89, No. 5, 997.

25. Cohen, R.S., Spitzer, L. and McR. Routly, P. (1950). The Electrical Conductivity of an Ionised Gas. Phys. Rev. 80, No. 2, 230.

26. Kovitya, P. and Lowke, J.J. (1985). Two-dimensional Analysis of Free-burning Arcs in Argon. J. Phys. D: Appl. Phys. 18, 53.

27. Kovitya, P. and Simpson, S.W. (1984). Non-equilibrium of Wall-stabilised AC Arcs at Low Currents. J. Phys. D: Appl. Phys. 17, 1829.

28. Kovitya, P. and Cram, L. (1983). Electrical Conductivity in Sun Spots and the Quiet Photosphere. J. Solar Phys. 84, 45.

29. Kowalenko, V. (1985). Examination of a Method for Predicting the Properties of Railgun Plasmas. Report MRL-R-960, Materials Research Laboratories, Melbourne, Victoria, Australia.

30. McNab, I.R. (1980). Electromagnetic Macroparticle Acceleration by a High Pressure Plasma. J. Appl. Phys. 51, 2549.

31. Rashleigh, S.C. and Marshall, R.A. (1978). Electromagnetic Acceleration of Macroparticles to High Velocities. J. Appl. Phys. 49, 2540.

32. Bedford, A.J. (1984). Rail Damage and Armature Parameters for Different Railgun Rail Materials. IEEE Transactions on Magnetics Vol. MAG-20, No. 2, 352.

33. Sadedin, D.R. and Stainsby, D.F. Experimental Investigation of a Three-Stage Railgun Incorporating Puff-Switching. Report MRL-R-1056, Materials Research Laboratories, Melbourne, Victoria, Australia.

34. Stainsby, D.F. and D.R. Sadedin, Experiments with a Small Injected Railgun. Report MRL-R-1055, Materials Research Laboratories, Melbourne, Victoria, Australia.

35. Powell, J.D. (1984). Thermal Energy Transfer from Arc to Rails in an Arc-Driven Rail Gun. IEEE Transactions on Magnetics Vol. MAG-20, No. 2, 395.

36. Kerrisk, J.F. (1981). Current Distribution and Inductance Calculations for Rail Gun Conductors. LA-9092-MS, LANL, New Mexico, USA.

37. Batteh, J.H. (1981). Analysis of a Rail Gun Plasma Accelerator, Report No. DAAK11-80-(0102), Science Applications Inc., Georgia, USA.

38. Bedford, A.J. (1984). Plasma Mass and Effective Inductance in a Small Railgun. Report MRL-R-947, Materials Research Laboratories, Melbourne, Victoria, Australia.

TABLE 1

Observations from the Streak Photographs of the RPIP Series

RPIP Shot	Type and Mass of Foil Used	Gunbody Used (No.)	Runaway Produced	Plasma Leakage	Plasma Breakup
1	Al, 0.0117 g	2	No	Yes	Yes
2	Al, 0.0117 g	1	No	No	No
3	Zn, 0.0422 g	2	Yes	No	Yes
4	Zn, 0.0422 g	1	No	No	No
5	Cu, 0.0510 g	2	No	No	No
6	Cu, 0.0475 g	1	No	No	No
7	Zn, 0.0083 g	2	Yes	No	No
8	Zn, 0.0086 g	1	Yes	No	No
9	Cu, 0.0127 g (0.009 g more likely)	1	No	Yes	No
10	Cu, 0.0079 g (0.009 g more likely)	2	Yes	Yes	No
11	Al, 0.0612 g	2	No	No	Yes
12	Al, 0.0615 g	1	No	No	Yes
13	Zn, 0.2126 g	2	No	Yes	Yes
14	Cu, 0.1976 g	2	No	Streak film lost	
15	Cu, 0.1960 g	1	No	No	Yes
16	Zn, 0.2006 g	2	No	No	Yes
17	Al, 0.0025 g	1	Yes	No	No
18	Al, 0.0024 g	2	Yes	No	No
19	Al, 0.0122 g	1	Yes	No	No
20	Al, 0.0120 g	2	Yes	No	No
21	Cu, 0.1972 g	1 (Reversed)	No	No	Yes
22	Zn, 0.0082 g	2 (Reversed)	No	Yes	No
23	Cu, 0.0069 g	1 (Reversed)	Streak photograph poor		
24	Al, 0.0024 g	2 (Reversed)	No	Streak photograph poor	
25	Al, 0.0118 g	1 (Reversed)	Yes	Yes	Streak incomplete
26	Cu, 0.0088 g	2 (Reversed)	Yes	Yes	No

TABLE 2

Exit Velocities for the RPIP Series

Shot RPIP	Flash/Beam (m/s)	Beam/Break (m/s)	Break/Pend (m/s)	Beam/Pend (m/s)	Pend (m/s)	Comments
Midpoint from muzzle	18 cm	36.2 cm	101.3 cm	98 cm		
1	1304+	775	742		---	Very small muzzzle flash. No pendulum trace
2	923	970+	860		595	
3	423+	928+	750		489	Early muzzle flash
4	946+	878+	891		616	Poor muzzle flash
5	---	---	---	733	290+	No definite muzzle flash. Two holes in the pendulum Missed pencil lead
6	898	---	---	841	602	Missed pencil lead. Two holes in pendulum
7	659	---	---	575	397+	Missed pencil lead. Two muzzle flashes
8	702	602	581		404	Two muzzle flashes
9	---	---	---		552	No data
10	316+	576+	713		496	Early muzzle flash. Possible fragmentation of projectile
11	405+	663+	773		489	Early and weak muzzle flash. Fragmented projectile
12	920	849	835		609	Two muzzle flashes
13	1345+	738	---		---	Two muzzle flashes. Missed pendulum
14	862	796	783		581	
15	880	840	833		623	
16	882	845	836		609	Possible fragmentation
17	789	709	694		474	Two muzzle flashes. Fragmentation (2 holes in pendulum)

TABLE 2
(continued)

Shot RPIP	Flash/Beam (m/s)	Beam/Break (m/s)	Break/Pend (m/s)	Beam/Pend (m/s)	Pend (m/s)	Comments
18	718	650	---		453	Break screen failed to register
19	731	---	---	811+	439	Two muzzle flashes. Missed pencil lead
20	688	610	596		411	Two muzzle flashes
21	993	962	956		730+	Marker pen not reliable
22	831	778	766		517	
23	---	---	---		545	No electronic record due to crowbar-switch failure.
24	893	774	766		439	Fragmented projectile
25	280+	508	---		---	Two muzzle flashes. Projectile missed pendulum
26	438+	625+	695		481	Two muzzle flashes. Possible fragmentation

The velocities marked with a '+' above them represent the most dubious of the results.

TABLE 3

Results for ω, L_o, τ and L_o/τ obtained from the analysis of the current-time records of the RPIP series

RPIP Shot	Angular Resonant Frequency ω(x 10^3 rad/s)	External Inductance L_o (μH)	Time Constant τ(x 10^{-4} sec)	Circuit Resistance L_o/τ (mΩ)
1	9.9 ± 0.2	6.4 ± 0.4	Insufficient current-time data	
2	9.9 ± 0.2	6.4 ± 0.4	8.3 ± 0.8	7.7 ± 1.2
3	9.8 ± 0.2	6.5 ± 0.4	8.6 ± 0.9	7.5 ± 1.3
4	10.0 ± 0.2	6.3 ± 0.3	8.5 ± 0.9	7.4 ± 1.3
5	9.8 ± 0.2	6.5 ± 0.3	8.1 ± 0.8	7.9 ± 1.3
6	Current-time data lost in transfer			
7	No current-time record			
8	Current-time data lost in transfer			
9	10.0 ± 0.2	6.2 ± 0.3	7.6 ± 0.8	8.2 ± 1.2
10	9.8 ± 0.2	6.5 ± 0.3	8.5 ± 0.9	7.6 ± 1.3
11	9.9 ± 0.2	6.4 ± 0.3	8.2 ± 0.8	7.7 ± 1.2
12	10.2 ± 0.2	6.0 ± 0.3	7.5 ± 0.8	8.0 ± 1.2
13	10.1 ± 0.2	6.1 ± 0.3	8.1 ± 0.8	7.6 ± 1.2
14	No current-time record			
15	9.9 ± 0.2	6.3 ± 0.3	8.8 ± 0.9	7.2 ± 1.2
16	10.0 ± 0.2	6.2 ± 0.3	8.3 ± 0.8	7.5 ± 1.2
17	9.8 ± 0.2	6.5 ± 0.3	8.7 ± 0.9	7.4 ± 1.3
18	9.9 ± 0.2	6.3 ± 0.3	7.2 ± 0.7	8.8 ± 1.4
19	9.9 ± 0.2	6.3 ± 0.3	7.9 ± 0.8	8.0 ± 1.3
20	9.9 ± 0.2	6.3 ± 0.3	7.2 ± 0.2	8.8 ± 1.4
21	No current-time record			
22	9.8 ± 0.2	6.5 ± 0.3	7.2 ± 0.7	9.0 ± 1.4
23	Current-time data different			
24	9.9 ± 0.2	6.3 ± 0.3	8.4 ± 0.8	7.5 ± 1.2
25	10.0 ± 0.2	6.2 ± 0.3	7.7 ± 0.8	8.1 ± 1.3
26	10.0 ± 0.2	6.3 ± 0.3	7.6 ± 0.8	8.3 ± 1.3

TABLE 4

Coefficients of Projectile Displacement vs Time Curves for the RPIP Series

RPIP Shot	Power of Time	Coefficients of Quadratic Displacement-Time Curve	Correlation Coefficient for Quadratic (p)	Coefficients of Cubic Displacement-Time Curve	Correlation Coefficient for Cubic (p)
1	t^3			$(-2.6 \pm 0.3) \times 10^{0}$ m/s^3	
	t^2	$(4.0 \pm 0.1) \times 10^{5}$ m/s^2		$(7.5 \pm 0.4) \times 10^{5}$ m/s^2	
	t^1	$(1.5 \pm 0.1) \times 10^{2}$ m/s		$(3.1 \pm 0.2) \times 10^{1}$ m/s	
	t^0	$(-9.8 \pm 2.0) \times 10^{-3}$ m		$(-2.8 \pm 1.4) \times 10^{-3}$ m	
			1.00		1.00
2	t^3			$(-1.5 \pm 0.5) \times 10^{8}$ m/s^3	
	t^2	$(5.6 \pm 0.1) \times 10^{5}$ m/s^2		$(7.4 \pm 0.6) \times 10^{5}$ m/s^2	
	t^1	$(1.5 \pm 0.1) \times 10^{2}$ m/s		$(8.5 \pm 2.2) \times 10^{1}$ m/s	
	t^0	$(-9.5 \pm 1.9) \times 10^{-3}$ m		$(-4.3 \pm 2.4) \times 10^{-3}$ m	
			1.00		1.00
3	t^3			$(-2.6 \pm 0.6) \times 10^{8}$ m/s^3	
	t^2	$(4.0 \pm 0.2) \times 10^{5}$ m/s^2		$(7.3 \pm 0.8) \times 10^{5}$ m/s^2	
	t^1	$(2.0 \pm 0.2) \times 10^{2}$ m/s		$(9.2 \pm 2.9) \times 10^{1}$ m/s	
	t^0	$(-1.1 \pm 2.8) \times 10^{-3}$ m		$(-3.9 \pm 2.8) \times 10^{-3}$ m	
					1.00
4	t^3			$(-4.1 \pm 0.3) \times 10^{8}$ m/s^3	
	t^2	$(5.6 \pm 0.2) \times 10^{5}$ m/s^2		$(1.06 \pm 0.04) \times 10^{6}$ m/s^2	
	t^1	$(1.4 \pm 0.1) \times 10^{2}$ m/s		$(-2.0 \pm 1.5) \times 10^{1}$ m/s	
	t^0	$(-1.1 \pm 0.3) \times 10^{-2}$ m		$(-1.0 \pm 1.4) \times 10^{-3}$ m	
			1.00		1.00
5	t^3			$(-2.3 \pm 0.3) \times 10^{8}$ m/s^3	
	t^2	$(4.3 \pm 0.1) \times 10^{5}$ m/s^2		$(7.4 \pm 0.3) \times 10^{5}$ m/s^2	
	t^1	$(1.28 \pm 0.01) \times 10^{2}$ m/s		$(2.0 \pm 1.3) \times 10^{1}$ m/s	
	t^0	$(-3.5 \pm 2.0) \times 10^{-3}$ m		$(3.2 \pm 1.3) \times 10^{-3}$ m	
			1.00		1.00
6	t^3			$(-2.0 \pm 0.5) \times 10^{8}$ m/s^3	
	t^2	$(5.8 \pm 0.1) \times 10^{5}$ m/s^2		$(8.\_ \pm 0.5) \times 10^{5}$ m/s^2	
	t^1	$(1.25 \pm 0.09) \times 10^{2}$ m/s		$(6.1 \pm 1.7) \times 10^{1}$ m/s	
	t^0	$(-0.7 \pm 1.4) \times 10^{-3}$ m		$(2.1 \pm 1.3) \times 10^{-3}$ m	
			1.00		1.00
7	t^3			$(-3.6 \pm 0.2) \times 10^{8}$ m/s^3	
	t^2	$(1.5 \pm 0.1) \times 10^{5}$ m/s^2		$(\ldots5 \pm 0.4) \times 10^{5}$ m/s^2	
	t^1	$(3.0 \pm 0.2) \times 10^{2}$ m/s		$(3.0 \pm 1.7) \times 10^{1}$ m/s	
	t^0	$(-2.9 \pm 0.4) \times 10^{-2}$ m		$(-2.4 \pm 2.1) \times 10^{-3}$ m	
			1.00		1.00

TABLE 4
(continued)

RPIP Shot	Power of Time	Coefficients of Quadratic Displacement-Time Curve	Correlation Coefficient for Quadratic (p)	Coefficients of Cubic Displacement-Time Curve	Correlation Coefficient for Cubic (p)
9	t^3			$(-5.9 \pm 0.3) \times 10^{8}$ m/s^3	
	t^2	$(5.3 \pm 0.2) \times 10^{5}$ m/s^2		$(1.25 \pm 0.03) \times 10^{6}$ m/s^2	
	t^1	$(1.6 \pm 1.4) \times 10^{1}$ m/s		$(-7.3 \pm 1.1) \times 10^{1}$ m/s	
	t^o	$(-1.3 \pm 0.3) \times 10^{-2}$ m/s		$(1.5 \pm 1.0) \times 10^{-3}$ m	
			1.00		1.00
10	t^3			$(-2.1 \pm 0.2) \times 10^{8}$ m/s^3	
	t^2	$(3.27 \pm 0.08) \times 10^{5}$ m/s^2		$(6.2 \pm 0.3) \times 10^{5}$ m/s^2	
	t^1	$(2.17 \pm 0.07) \times 10^{2}$ m/s		$(1.1 \pm 0.1) \times 10^{2}$ m/s	
	t^o	$(-1.5 \pm 0.2) \times 10^{-2}$ m		$(-6.0 \pm 1.3) \times 10^{-3}$ mj	
			1.00		1.00
11	t^3			$(-4.7 \pm 0.4) \times 10^{8}$ m/s^3	
	t^2	$(4.4 \pm 0.2) \times 10^{5}$ m/s^2		$(1.02 \pm 0.06) \times 10^{6}$ m/s^2	
	t^1	$(2.3 \pm 0.1) \times 10^{2}$ m/s		$(4.2 \pm 2.0) \times 10^{1}$ m/s	
	t^o	$(-1.9 \pm 0.3) \times 10^{-2}$ m		$(-3.7 \pm 2.2) \times 10^{-3}$ m	
			1.00		1.00
12	t^3			$(-3.0 \pm 0.3) \times 10^{8}$ m/s^3	
	t^2	$(5.1 \pm 0.1) \times 10^{5}$ m/s^2		$(8.8 \pm 0.3) \times 10^{5}$ m/s^2	
	t^1	$(1.6 \pm 0.1) \times 10^{2}$ m/s		$(4.4 \pm 1.1) \times 10^{1}$ m/s	
	t^o	$(-8.3 \pm 1.9) \times 10^{-3}$ m		$(-1.1 \pm 0.1) \times 10^{-3}$ m	
			1.00		1.00
13	t^3			$(-2.5 \pm 0.7) \times 10^{8}$ m/s^3	
	t^2	$(4.5 \pm 0.2) \times 10^{5}$ m/s^2		$(7.6 \pm 0.9) \times 10^{5}$ m/s^2	
	t^1	$(1.8 \pm 0.1) \times 10^{2}$ m/s		$(8.0 \pm 3.0) \times 10^{1}$ m/s	
	t^o	$(-1.2 \pm 0.2) \times 10^{-2}$ m		$(-5.3 \pm 2.8) \times 10^{-3}$ m	
			1.00		1.00
15	t^3			$(-3.6 \pm 0.4) \times 10^{8}$ m/s^3	
	t^2	$(5.0 \pm 0.1) \times 10^{5}$ m/s^2		$(9.6 \pm 0.5) \times 10^{5}$ m/s^2	
	t^1	$(1.5 \pm 0.1) \times 10^{2}$ m/s		$(-0.4 \pm 1.8) \times 10^{-2}$ m/s	
	t^o	$(-8.9 \pm 2.2) \times 10^{-3}$ m		$(0.2 \pm 1.6) \times 10^{-3}$ m	
			1.00		1.00
26	t^3			$(-2.1 \pm 0.2) \times 10^{8}$ m/s^3	
	t^2	$(3.0 \pm 1.0) \times 10^{5}$ m/s^2		$(6.8 \pm 0.4) \times 10^{5}$ m/s^2	
	t^1	$(2.93 \pm 0.09) \times 10^{2}$ m/s		$(1.6 \pm 0.1) \times 10^{2}$ m/s	
	t^o	$(-1.40 \pm 0.2) \times 10^{-2}$ m		$(-5.0 \pm 1.3) \times 10^{-3}$ m	
			1.00		1.00

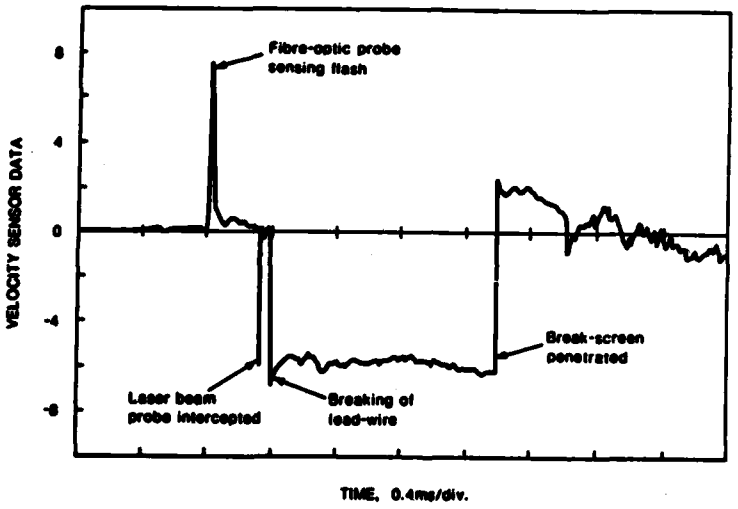

FIGURE 1 Time-of-arrival Record for RPIP02

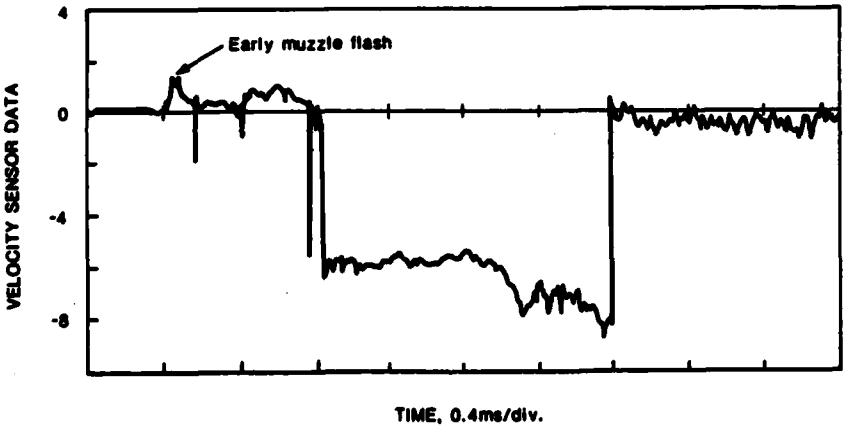

FIGURE 2 Time-of-arrival Record for RPIP11

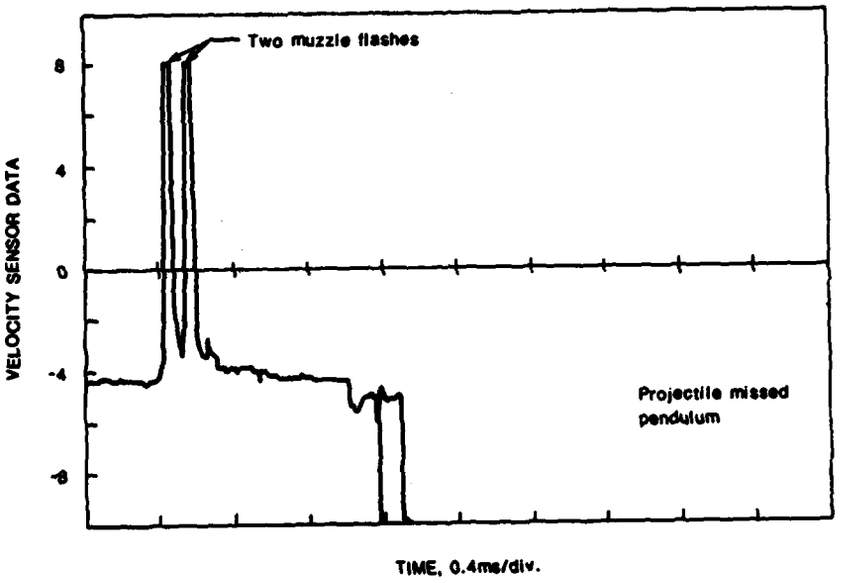

FIGURE 3 Time-of-arrival Record for RPIP25

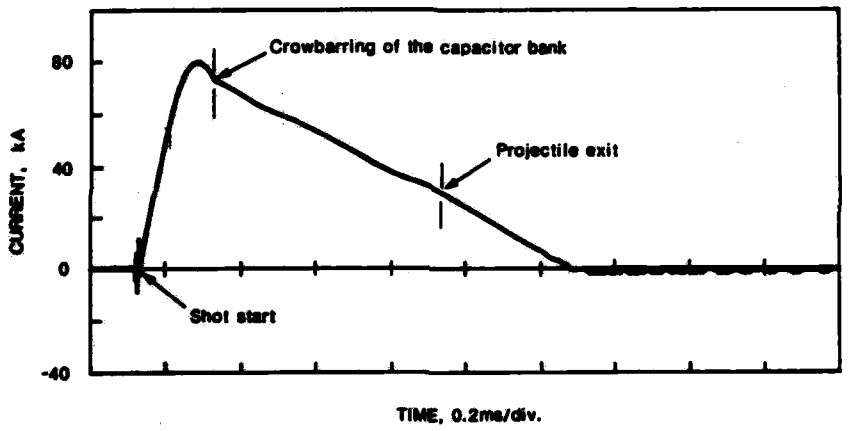

FIGURE 4 Current-time Record for RPIP02

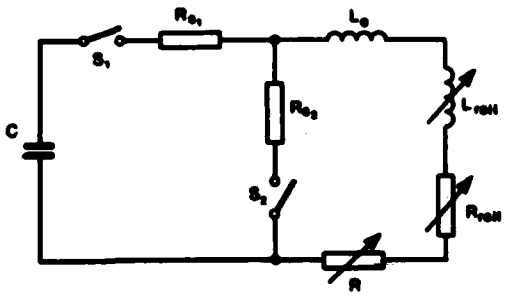

FIGURE 5 Electric Circuit for a RAPID Railgun

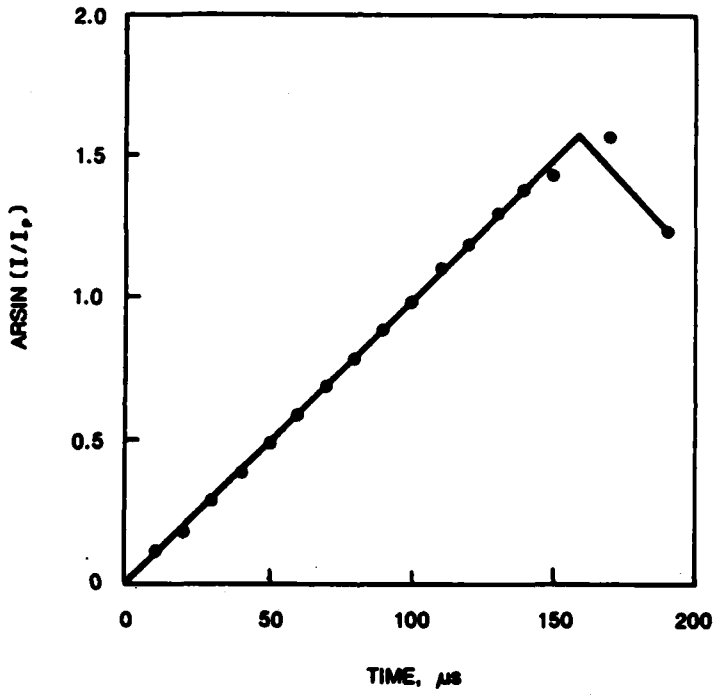

FIGURE 6 Arsin (I/I_p) vs Time for RPIP02 (pre-crowbar)

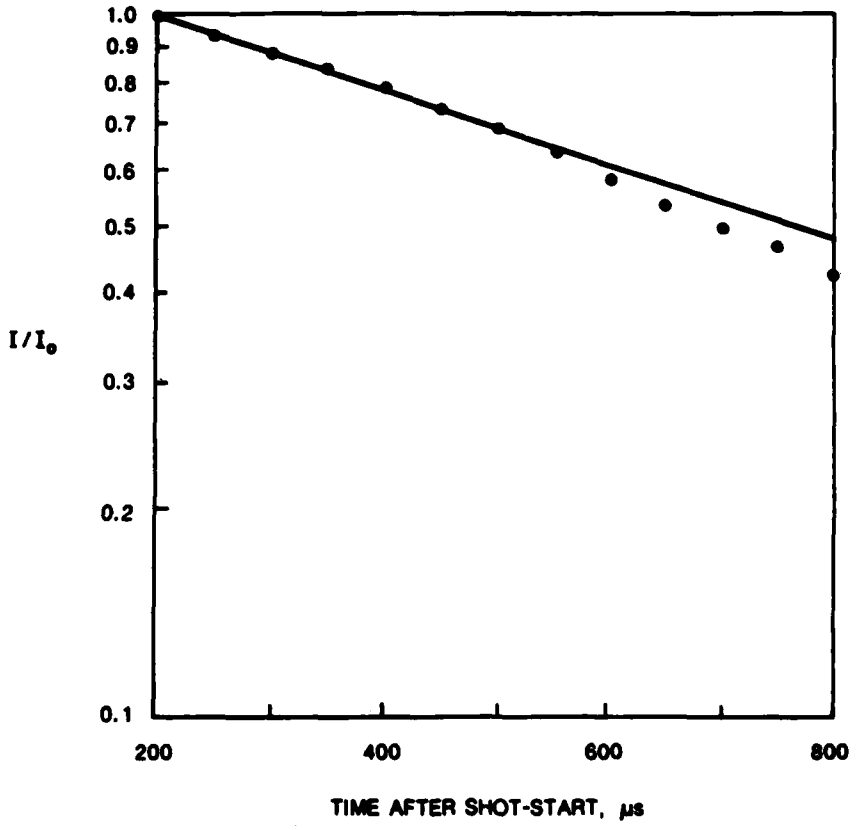

FIGURE 7 I/I_o versus Time for RPIP02 on a Log-linear Scale

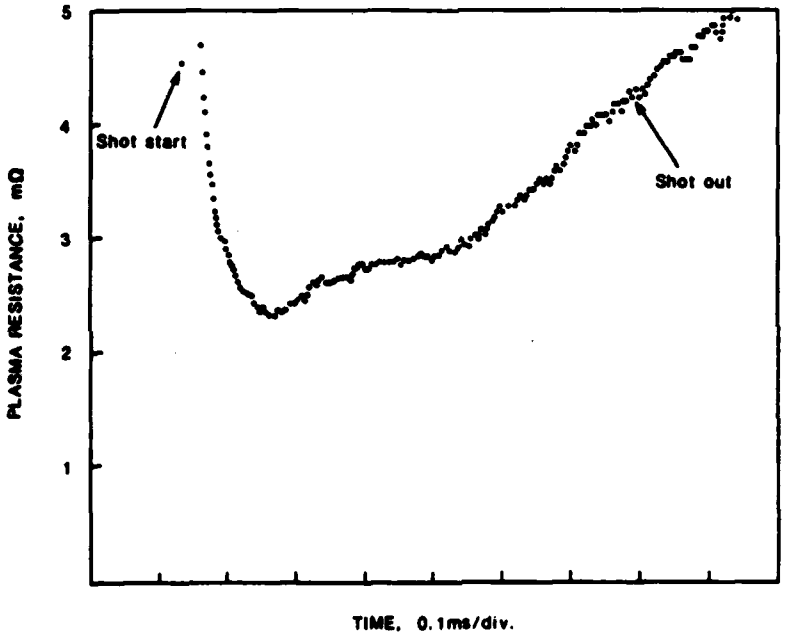

FIGURE 8 Plasma Armature Resistance versus Time for RPIP02

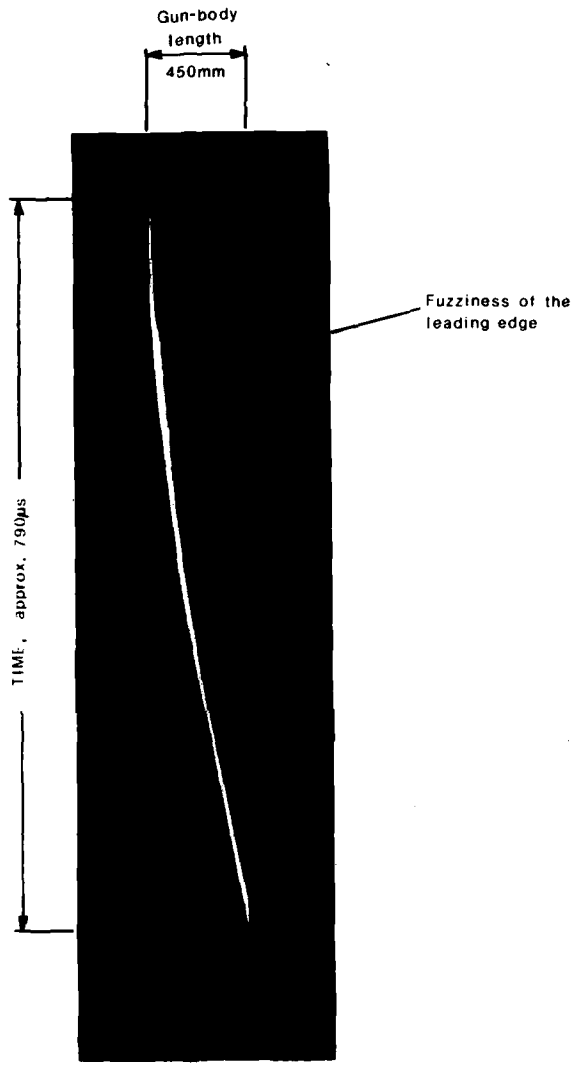

FIGURE 9 Streak Photograph for RPIP02 (Time is measured vertically downwards and displacement is measured horizontally to the right)

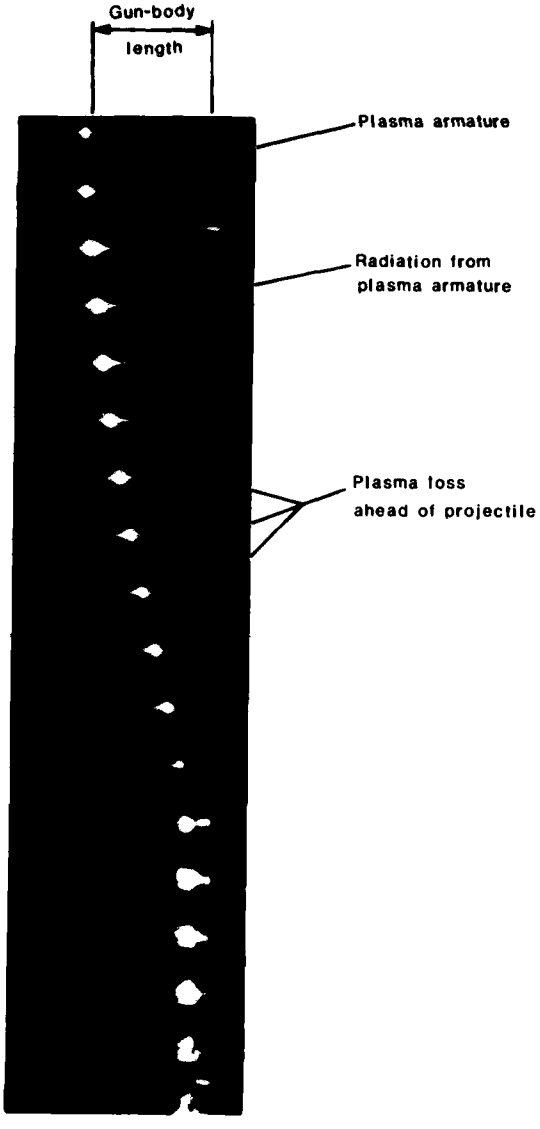

FIGURE 10 Framing Photograph for RPIP02

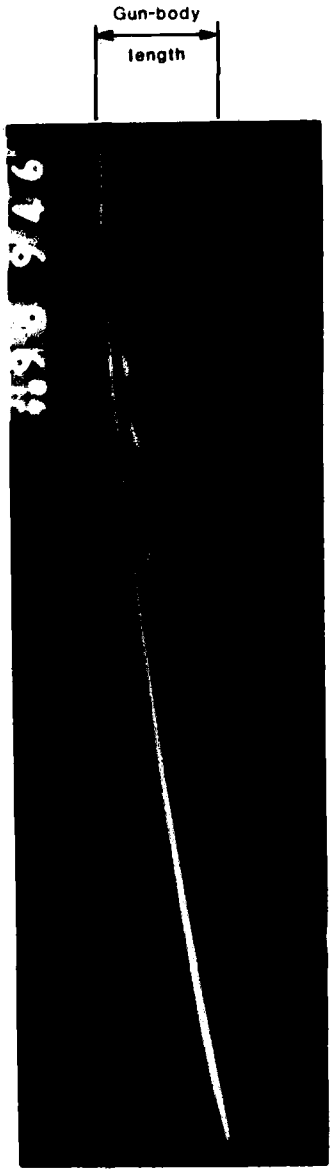

FIGURE 11 Streak Photograph for RPIP01

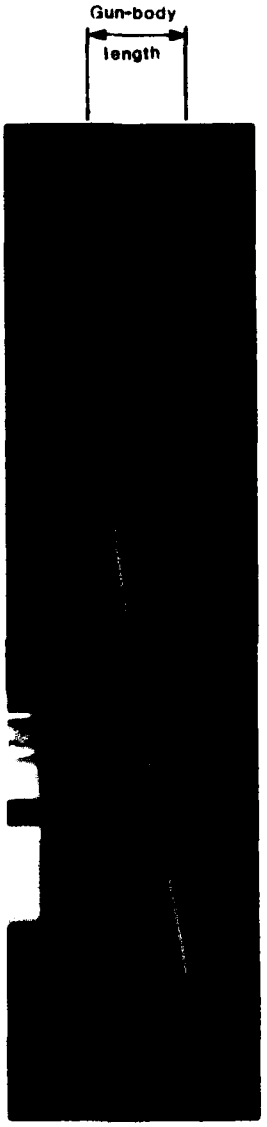

FIGURE 12 Streak Photograph for RPIP15

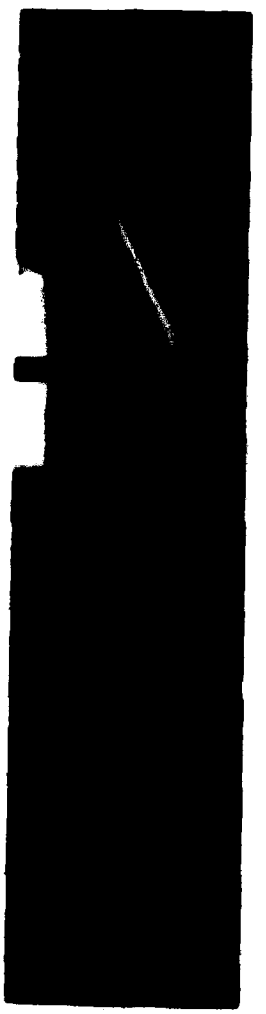

FIGURE 13 Streak Photograph for RPIP19

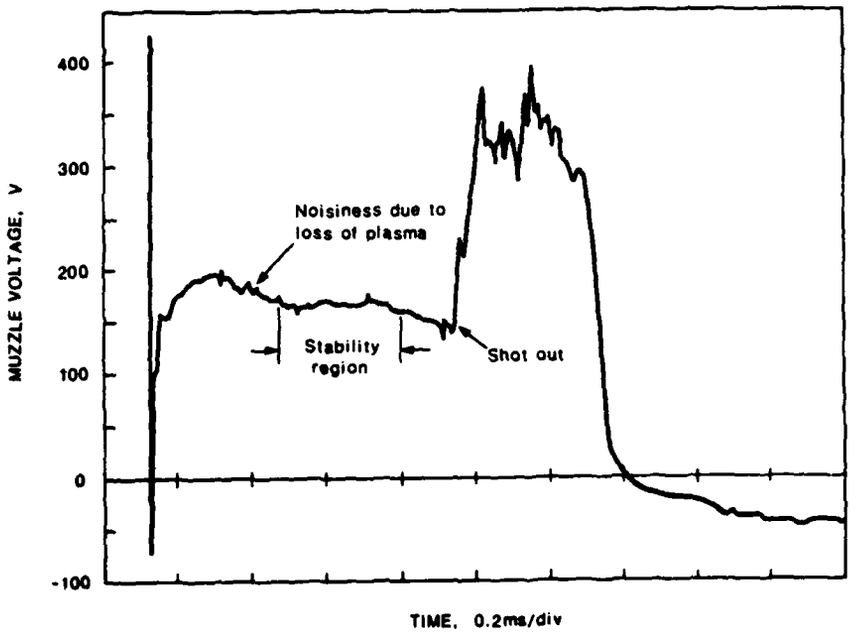

FIGURE 14 Muzzle Voltage Record for RPIP02

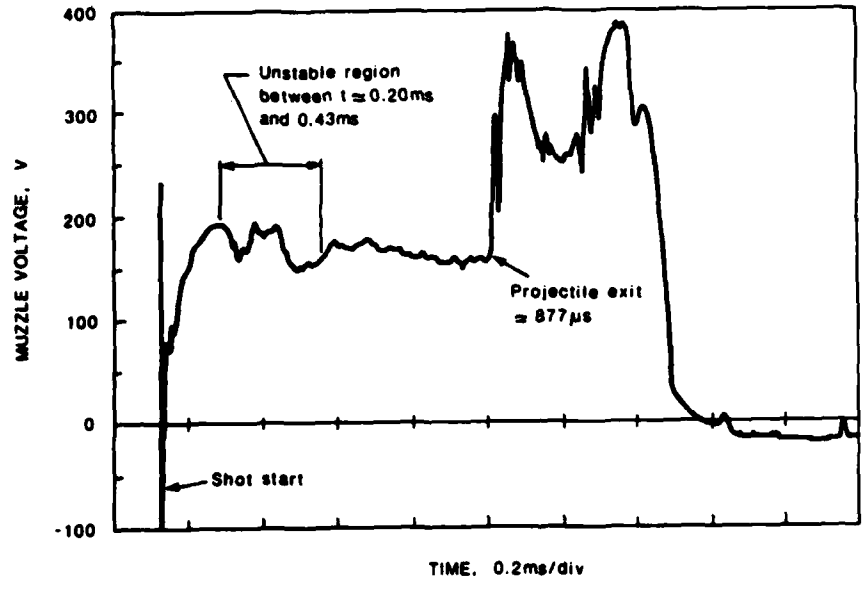

FIGURE 15 Muzzle Voltage Record for RPIP15

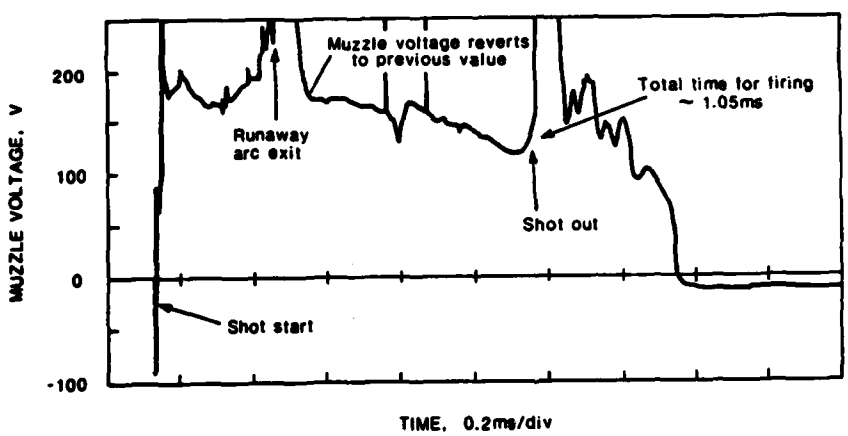

FIGURE 16 Muzzle Voltage Record for RPIP19

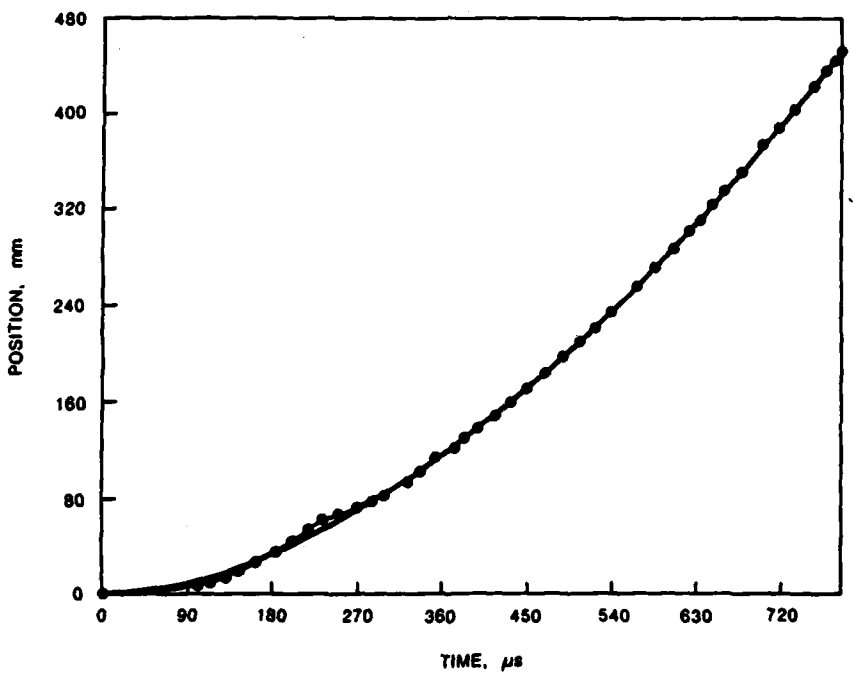

FIGURE 17 Position versus Time for RPIP02

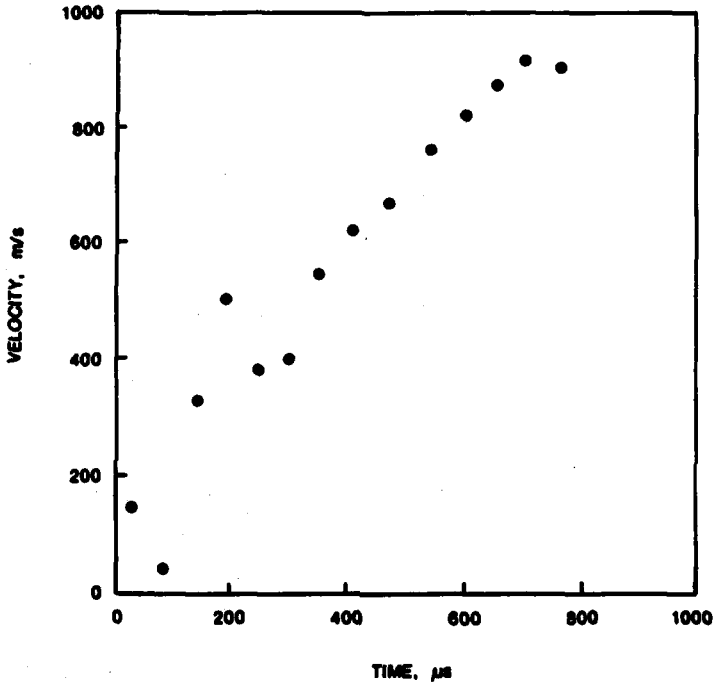

FIGURE 18 Velocity versus Time for RPIP02

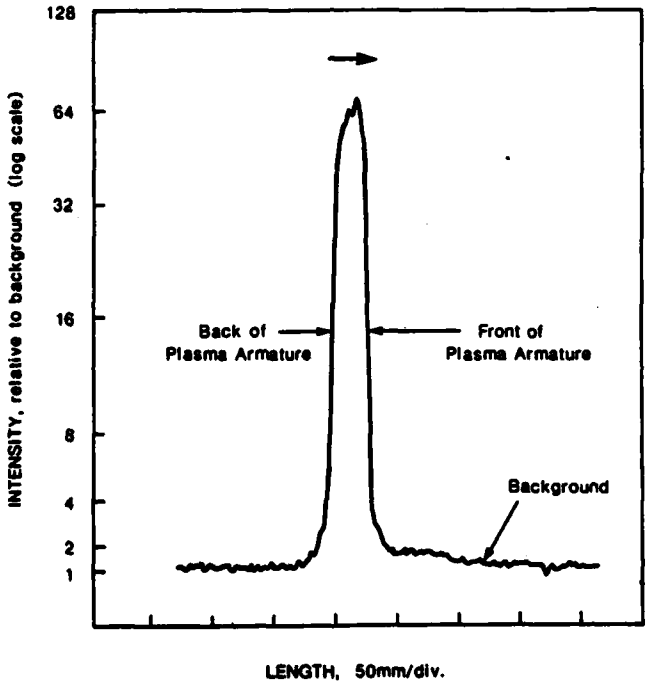

FIGURE 19 Plasma Intensity Profile for RPIP02 about 3.4×10^2 μs after Plasma Initiation

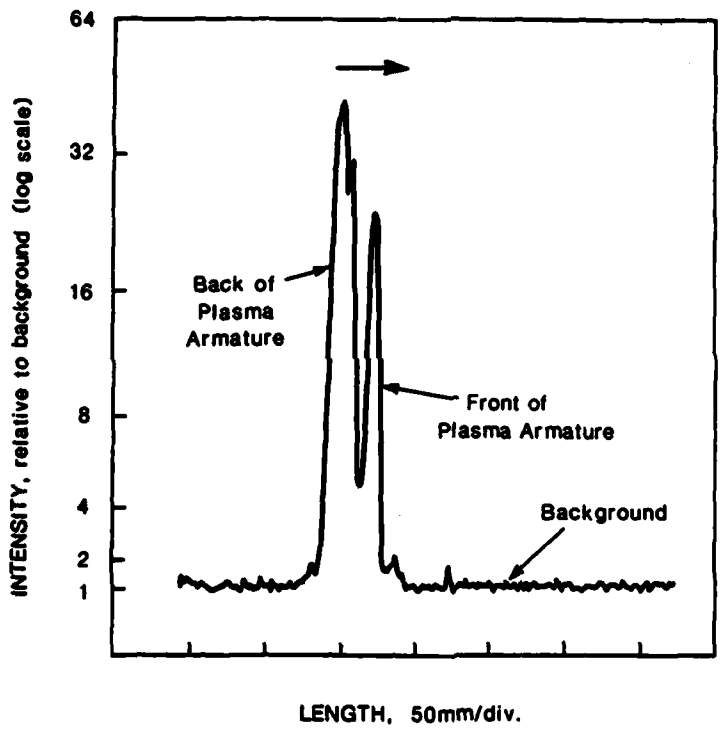

FIGURE 20 Plasma Intensity Profile for RPIP02 about 2.2×10^2 μs after Plasma Initiation

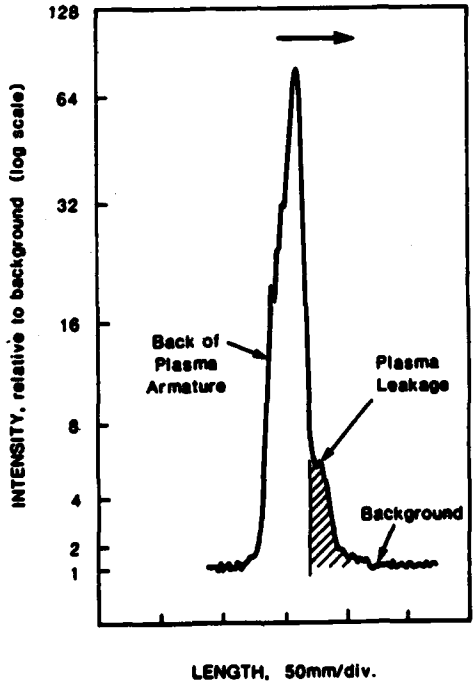

FIGURE 21 Plasma Intensity Profile for RPIP02 between 2.2 x 10^2 μs and 3.4 x 10^2 μs after Plasma Initiation

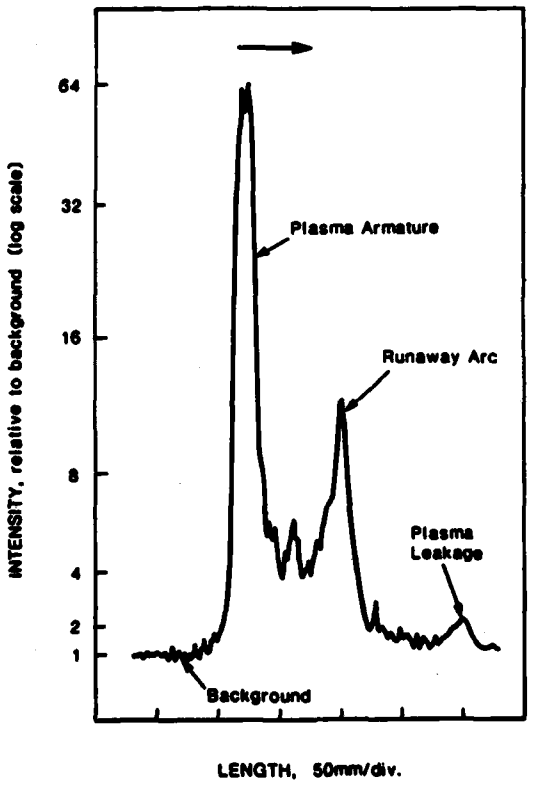

FIGURE 22 Formation of a Runaway Arc for RPIP26

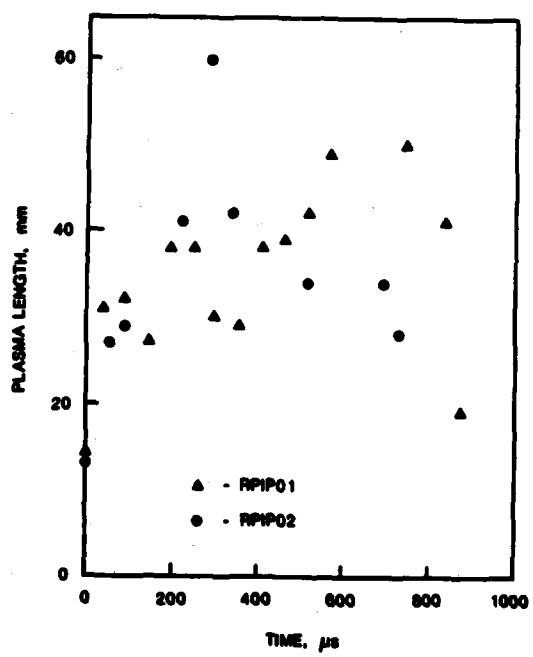

FIGURE 23 Plasma Length vs Time for RPIP01 and RPIP02

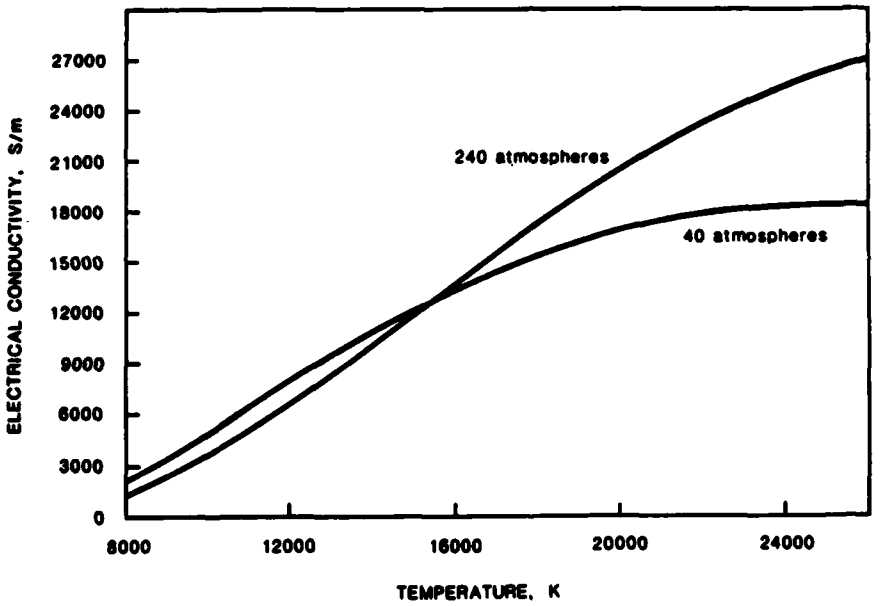

FIGURE 24 Electrical Conductivity of a Copper Plasma vs. Temperature
1 - 40 atm. 2 - 240 atm.

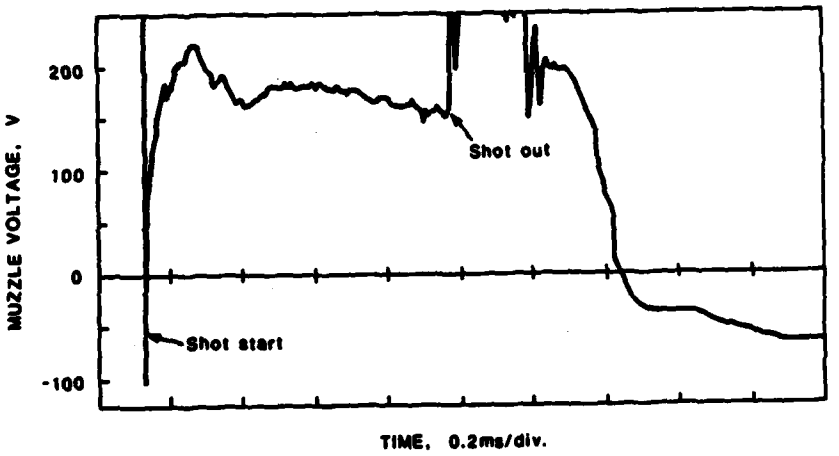

FIGURE 25 Muzzle Voltage Record for RPIP06

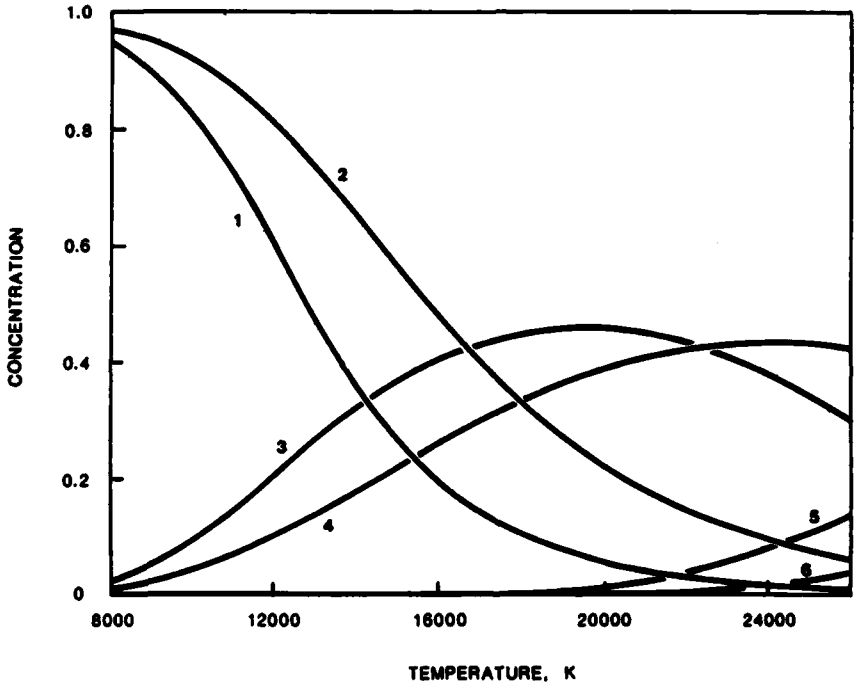

FIGURE 26 Concentration of Copper Species vs. Temperature

1 - Cu at 40 atm. 2 - Cu at 240 atm.
3 - Cu^{+} at 40 atm. 4 - Cu^{+} at 250 atm.
5 - Cu^{2+} at 40 atm. 6 - Cu^{2+} at 240 atm.

APPENDIX

THE SOLUTION OF KIRCHHOFF'S EQUATION WITH $L_o/R_1 = L'/R'$

In this appendix it is shown that a solution to Kirchhoff's equation given by Equation (18) can be obtained without a knowledge of the projectile displacement x(t) and railgun current I only when $L_o/R_1 = L'/R'$ where R_1 is the sum of R and R_{S_2} and is assumed to be constant. Assuming that L_o, L' and R' are also constant, Equation (18) can be written as:

$$L_o e^{-R_1 t/L_o} \frac{d}{dt}\left(I\, e^{R_1 t/L_o}\right) = -L' e^{-R't/L'} \frac{d}{dt}\left(I \times e^{R't/L'}\right) \qquad (A\text{-}1)$$

Multiplying Equation (A-1) by $\exp(R't/L')$ and then integrating with respect to time from t_c yields:

$$-L'\left(I \times e^{R't/L'} - I(t_c)x(t_c)e^{R't_c/L'}\right) = \int_{t_c}^{t} L_o\, e^{(R'/L'-R_1/L_o)t} \frac{d}{dt}\left(I\, e^{R_1 t/L_o}\right) dt \qquad (A\text{-}2)$$

The integral on the right hand side of Equation (A-2) can be evaluated without a knowledge of I only when the time constant associated with the rails (L'/R') is equal to the time constant associated with the external railgun circuit (L_o/R_1). When this condition holds, Equation (A-2) becomes:

$$I \times e^{R't/L'} = I(t_c)x(t_c)e^{R't_c/L'} - \frac{L_o}{L'}\left(I\, e^{R_1 t/L_o} - I(t_c)e^{R_1 t_c/L_o}\right) \qquad (A\text{-}3)$$

An alternative form of Equation (A-3) is:

$$I = \frac{I(t_c)(x(t_c) + L_o/L')}{(x + L_o/L')} \exp(-(R_1(t - t_c)/L_o) \qquad (A\text{-}4)$$

As expected, Equation (A-4) reduces to Equation (20) when $x << L_o/L'$ and when $x >> L_o/L'$, Equation (A-4) reduces to Equation (21).

SECURITY CLASSIFICATION OF THIS PAGE **UNCLASSIFIED**

DOCUMENT CONTROL DATA SHEET

REPORT NO.	AR NO.	REPORT SECURITY CLASSIFICATION
MRL-R-1053	AR-005-131	Unclassified

TITLE

Analysis of a series of electromagnetic launcher firings

AUTHOR(S)

V. Kowalenko

CORPORATE AUTHOR

Materials Research Laboratories
PO Box 50,
Ascot Vale, Victoria 3032

REPORT DATE	TASK NO.	SPONSOR
June 1987	DST 82/212	DSTO

FILE NO.	REFERENCES	PAGES
G6/4/8-3210	38	94

CLASSIFICATION/LIMITATION REVIEW DATE	CLASSIFICATION/RELEASE AUTHORITY
February 1990	Superintendent, MRL Physics Division

SECONDARY DISTRIBUTION

Approved for Public Release

ANNOUNCEMENT

Announcement of this report is unlimited.

KEYWORDS

Railgun
Electromagnetic
Accelerators
Launchers

SUBJECT GROUPS 0081B 0046G 0079G

ABSTRACT

In this report theoretical aspects of electromagnetic launchers are presented in conjunction with an analysis of diagnostic measurements taken during the RAPID Plasma Intensity Profiles (RPIP) series of firings. These theoretical aspects deal with the current-time behaviour, the plasma temperature and the evaluation of railgun parameters such as the efficiency and effective inductance per unit length.

The principal aims of the RPIP series were: (1) to see if different types and masses of plasma-generating foils affected railgun performance and the diagnostic measurements taken during each firing and (2) to compare some of the theoretical predictions of the Plasma Armature Rail Accelerator (PARA) simulation code with experimental results.

Projectile displacement-time results for the series were obtained by digitising photographs from a streak camera and in order to verify the PARA predictions for plasma-length behaviour, light intensity profiles were produced from microdensitometer readings of the streak films.

The experimental results were affected by plasma disruption, arcing ahead of the projectile and plasma leakage. These effects are also discussed in this report.

END

DATE
FILMED

3 85